Received: 12 October 2020 | Revised: 25 November 2020 | Accepted: 6 December 2020

DOI: 10.1002/cey2.99

REVIEW

CARBON ENERGY WILEY

Architecture engineering of carbonaceous anodes for high-rate potassium-ion batteries

Tianlai Wu[1,2] | Weicai Zhang[1,2] | Jiaying Yang[3] | Qiongqiong Lu[4] | Jing Peng[1,2] | Mingtao Zheng[1,2] | Fei Xu[3] | Yingliang Liu[1,2] | Yeru Liang[1,2]

[1]Key Laboratory for Biobased Materials and Energy of Ministry of Education, Guangdong Provincial Engineering Technology Research Center for Optical Agriculture, College of Materials and Energy, South China Agricultural University, Guangzhou, China

[2]Guangdong Laboratory of Lingnan Modern Agriculture, Guangzhou, China

[3]State Key Laboratory of Solidication Processing, School of Materials Science and Engineering, Center for Nano Energy Materials, Northwestern Polytechnical University and Shaanxi Joint Laboratory of Graphene (NPU), Xi'an, China

[4]Leibniz Institute for Solid State and Materials Research (IFW) Dresden e.V., Dresden, Germany

Correspondence
Fei Xu, State Key Laboratory of Solidication Processing, Center for Nano Energy Materials, School of Materials Science and Engineering, Northwestern Polytechnical University and Shaanxi Joint Laboratory of Graphene (NPU), 710072 Xi'an, China.
Email: feixu@nwpu.edu.cn

Yeru Liang, Key Laboratory for Biobased Materials and Energy of Ministry of Education, Guangdong Provincial Engineering Technology Research Center for Optical Agriculture, College of Materials and Energy, South China Agricultural University, 483 Wushan Rd, 510642 Guangzhou, China.
Email: liangyr@scau.edu.cn

Funding information
National Natural Science Foundation of China, Grant/Award Numbers: 51972121, 51972270, 51702262; Tip-top Scientific and Technical Innovative Youth Talents of Guangdong Special Support Program, Grant/Award Number: 2017TQ04C419; Key Research and Development Program of Shaanxi Province, Grant/Award Number: 2019TSLGY07-03;

Abstract

The limited lithium resource in earth's crust has stimulated the pursuit of alternative energy storage technologies to lithium-ion battery. Potassium-ion batteries (KIBs) are regarded as a kind of promising candidate for large-scale energy storage owing to the high abundance and low cost of potassium resources. Nevertheless, further development and wide application of KIBs are still challenged by several obstacles, one of which is their fast capacity deterioration at high rates. A considerable amount of effort has recently been devoted to address this problem by developing advanced carbonaceous anode materials with diverse structures and morphologies. This review presents and highlights how the architecture engineering of carbonaceous anode materials gives rise to high-rate performances for KIBs, and also the beneficial conceptions are consciously extracted from the recent progress. Particularly, basic insights into the recent engineering strategies, structural innovation, and the related advances of carbonaceous anodes for high-rate KIBs are under specific concerns. Based on the achievements attained so far, a perspective on the foregoing, and proposed possible directions, and avenues for designing high-rate anodes, are presented finally.

KEYWORDS

carbonaceous anodes, electronic conductivity, high-rate performance, ion diffusivity, potassium-ion batteries

Tianlai Wu, Weicai Zhang, and Jiaying Yang contributed equally to this study.

Guangdong Province Universities and Colleges Pearl River Scholar Funded Scheme, Grant/Award Number: 2017; Guangdong Basic and Applied Basic Research Foundation, Grant/Award Number: 2019A1515011502; Natural Science Foundation of Shaanxi Province, Grant/Award Number: 2020JZ-07

1 | INTRODUCTION

During the past decades, lithium-ion batteries (LIBs) have achieved great success for use in portable electronic devices, electric vehicles, and smart grid. Nevertheless, the limited abundance and uneven distribution of lithium resources in earth's crust hinder the sustainable development and further application of LIBs. To address this issue, development of alternative electrochemical energy storage systems composed of abundant elements such as sodium, potassium, aluminum, and magnesium has been intensively pursued. Among the various candidates, potassium-ion batteries (KIBs) are considered as a promising system in the benefit of resource-abundant of potassium element (2.4 wt% potassium in the Earth's crust), a low redox potential of the K^+/K redox couple (−2.93 V vs. standard hydrogen electrode) and similar energy storage mechanism to LIBs.[1–4] For application in scenarios or electric equipment that do not require high energy density, KIBs can supple or selectively replace LIBs to alleviate the shortage of lithium resources. In addition, KIBs have great application potential in large-scale energy storage systems due to their high cost effectiveness.

Despite the valuable advantages, the further development of KIBs is frustrated. One of the bottlenecks required to break through is their fast capacity fading at high rates. In general, the achievable charge/discharge rate of KIBs mainly depends on the migration rate of ions and electrons transfer within the battery, including electrodes, electrolytes, and their interfaces. Early studies have shown that K^+ has the higher ionic mobility and ionic conductivity in electrolytes because K^+ has a smaller Stokes' radius (3.6 Å) compared with Li^+ (4.8 Å).[5] However, it is still difficult to achieve satisfactory rate capability for KIBs due to the much larger diameter of K^+ (1.38 vs. 0.76 Å for Li^+), leading to poor solid-phase diffusion or intercalation/deintercalation kinetics and huge volume variation in the bulk electrode materials. This is especially notable in the anodes. Therefore, the key to design high-rate KIBs is the construction of suitable anode materials that are capable of smooth and fast potassiation/depotassiation with structural stability.

Up till now, significant efforts have been devoted to the design and fabrication of rational anode materials with diverse components, structures, and morphologies.[6,7] A large number of materials including metal oxides/sulfides/phosphides (e.g., SnO_2,[8] CuO,[9] Co_3O_4,[10] MoS_2,[11] SnS_2,[12] Sb_2S_3,[13] CoS,[14] CuP_2,[15] GeP_5,[16] and Sn_4P_3[17]), metals/alloys (e.g., Sn,[18] Sb,[19] Ge,[20] Bi,[21] and their alloys[22,23]), organic matters (e.g., ADAPTS,[24] H_2TP,[25] K_2TP,[26] K_2BPDC,[27] and $K_2C_6O_6$[28]), and carbonaceous materials (e.g., graphite,[29] graphene,[30] carbon nanotube [CNT],[31] and porous carbon[32]) have been explored to be utilized as anodes for KIBs. These emerging anode materials showed impressive K^+ storage capability, which can even compare favorably with those of LIBs. The metals/alloys and metal oxides/sulfides/phosphides anodes usually deliver large specific capacities and energy densities, but often suffer from large volume expansion during the charge/discharge process, resulting in inferior cycle stability and rate performance. Although organic matters used as KIBs anodes exhibit impressive electrochemical performances, they are poorly conductive. Furthermore, their synthesis usually involves complicated steps under rigorous conditions and/or expensive raw precursors, causing difficulties of large-scale production. In this context, carbonaceous materials turn out to be the most promising candidates because they are accompanied with excellent electronic conductivity, good physicochemical stability, versatile availability, low cost, and ease of processability. Over the past few years, various carbonaceous materials have been designed, prepared and utilized as anodes for KIBs through extensive theoretical and experimental studies.[33,34] However, the development of an ideal carbon anode for reversible and fast K^+ storage is so far in its infancy stage and understanding the underlying principles governing the K^+ storage behavior in carbon structure is still highly desirable. Although the progress in carbonaceous anodes for KIBs have been summarized and discussed in some impactful and in-depth reviews, rare of them focus on the strategies and approaches toward the achievement of high-rate KIBs.

In this review, we aim to present and highlight how architectural engineering of carbonaceous anodes gives rise to high-rate performances for KIBs, and also to consciously extract beneficial conceptions from these

progresses. We first describe two key parameters (e.g., electronic conductivity and ion diffusivity) that have profound impacts on the enhanced rate performance of anodes. Then, recent strategies and advances of carbonaceous anodes in achieving high-rate KIBs are introduced in detail. These strategies include design and construction of framework and morphology for carbonaceous anode materials related to a series of regulation and construction. Based on the achievements attained so far, a perspective on the foregoing, and proposed possible directions and avenues are presented. The strategies and prospects outlined in this review are intended to provide practical guidance for a growing number of researchers to explore the next generation of high-rate KIBs, and the mentioned methodology is expected to be applicable to the development of other energy storage systems as well.

2 | KEY PARAMETERS FOR HIGH-RATE PERFORMANCE

KIBs use a "rocking-chair"-type mechanism in the same manner that LIBs do, in which both cathode and anode materials employ topotactic intercalation chemistry for charge storage. To achieve high-rate performance of KIBs, it is important to understand the transport pathways and modes of K^+ and electrons in the whole battery systems, and to raise the diffusion kinetics during the rate-limiting step. Taking the discharge process as an example, the operation mechanism of KIBs is schematically illustrated in Figure 1.[35] (1) K^+ and electrons concurrently disassociate from anode material, in which K^+ transport is dominated by solid-state diffusion within electrode to the anode/electrolyte interface. (2) K^+ approaches the anode/electrolyte interface, and then diffuses into the electrolyte and migrates to the cathode side. (3) The electrons driven by a higher potential of cathode side pass through the anode particles and their interface toward the current collector, and migrate by the external circuit to supply power to equipment/device. (4) K^+ and electrons enter the cathode materials concurrently via solid-state diffusion.

According to the above operation mechanism, it illuminates that the rate performances of KIBs depend critically on the migration rate of the K^+ and electrons transfer within the electrodes, electrolytes, and their interfaces. Previous studies have shown that ions and electrons transport kinetics of electrodes, especially anodes, was considered to be the rate-determining step of working batteries.[36,37] Accordingly, the construction of suitable anodes is one of the core technologies for designing KIBs with high-rate performance. Specifically, electronic conductivity and ion diffusivity of anodes are two key parameters.

2.1 | Improvement of electronic conductivity

For realizing fast electron transport in anode materials, it is warranted to comprehend the conductive mechanism of electrons. Generally speaking, all solid anode materials follow the theory of solid energy band. According to this theory, stimulated electrons in the valence band cross forbidden band and enter conduction band, thereby realizing the conduction of the solid anode materials. The conductivity of solid anode materials is described as:

$$\sigma = ne\mu, \tag{1}$$

where σ is the electronic conductivity, n is the carrier concentration, and μ is the carrier mobility. Based on Equation (1), σ of the solid anode materials can be improved by increasing n or μ. For example, carbon materials usually exhibit high σ values because of their excellent μ. Another example is that metal or alloy materials with smaller bandgap or zero bandgap that allow electrons to easily cross the forbidden band usually show high σ values.

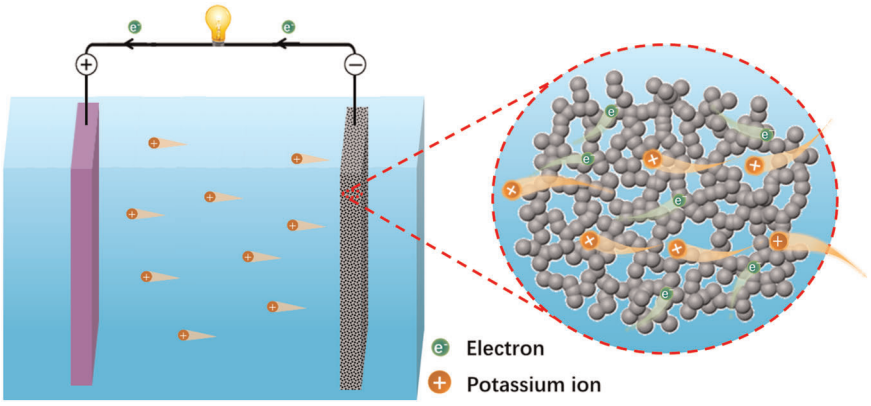

FIGURE 1 Transport pathways of the potassium ions and the electrons in the discharging process of KIBs

Considering the existence of holes and free electrons in solid anode materials, σ could be further described as shown in the following equation:

$$\sigma = n_i e\mu_e + p_i e\mu_h, \tag{2}$$

where n_i and p_i represent the concentrations of electrons and holes, respectively, and μ_e and μ_h represent the mobility of the electrons and the holes, respectively. Based on Equation (2), an increase in n_i and p_i enhances the conductivity of the solid anode materials. Heteroatom doping in carbon is capable of providing additional holes or electrons, and thus is an effective way to improve the σ of anode materials. In addition, the local electronic structure of the carbon materials could be adjusted by forming a strengthening bond between the doped heteroatom and carbon atom, thus affecting the conductivity.

2.2 | Improvement of ion diffusivity

The previous section has shown how to improve σ of the anode materials theoretically. However, in addition to σ, ion diffusivity (D_i) should be considered when designing high-rate performance in KIBs. A typical example is the zero-band-gap graphite. Graphite is often used as an anode material in batteries due to the extremely high σ (>1.0 S cm^{-1}) accompanied by low cost and excellent stability.[38–40] However, the narrow interlayer spacing (3.35 Å) of graphite and the long diffusion distance (several microns) of K^+ result in low D_i of graphite, which limits the rate performance of graphite in KIBs. It was shown that the commercial graphite delivered a low rate capacity of 8 mAh g^{-1} at 1 A g^{-1}.[41] Hence, it is certainly worth getting insight into the key factors affecting the D_i to achieve high-rate KIBs.

According to the Arenius equation, D_i is expressed according to the following equation:

$$D_i = D_0 \exp\left(-\frac{\Delta G}{k_B T}\right), \tag{3}$$

where ΔG is the energy barrier, k_B is the Boltzmann constant, and D_0 is the prefactor estimated empirically. It is found that increasing the working temperature (T) enhances D_i, but high temperature would easily lead to safety problems of batteries. From the practical considerations, a decrease in ΔG is a crucial way to raise D_i, which could be achieved by regulating the anode structure.[42] For K^+ diffusion in electrode materials, D_i could be also expressed in the following equation:

$$D_i = \frac{d^2}{\tau}. \tag{4}$$

Consequently, for the sake of enhancing D_i, it is essential to shorten the diffusion time (τ), or reduce the ion diffusion length (d) by using nanosize or porous structure materials.[43–46]

Based on the above discussion, two key parameters, electronic conductivity and ion diffusivity of anodes, have a profound influence on the rate performance of KIBs. Nevertheless, in the identical anode material, it is difficult to concurrently reach the maximum value of these two parameters. Thus, it is necessary and feasible to adjust these two parameters to achieve a balance for obtaining practical available high-rate KIBs. In recent years, many strategies and advances of high-rate KIBs using carbonaceous anodes have been reported. Most of these strategies were related to the framework and morphology design of carbonaceous materials, which can regulate electronic conductivity or ion diffusivity in different aspects to construct high-rate carbonaceous anodes.

3 | DESIGN OF FRAMEWORK

As we all know, the diffusion of electrons and ions in electrode rather than that in electrolyte is the kinetically limited step during electrochemical reaction, especially at high current density. To attain high-rate KIBs, the design of carbonaceous framework is a meaningful avenue because it promotes the transport of electrons and ions in carbonaceous anodes. Significant efforts have been devoted to designing the framework of carbonaceous anode materials through regulation of carbon microcrystal structure, heteroatoms doping and regulation of composition, which thus controlled the electronic conductivity and ion diffusivity of carbonaceous anodes to achieve high-rate KIBs (Figure 2).

3.1 | Regulation of carbon microcrystal structure

3.1.1 | Regulation of graphitic crystalline structure

The graphitization of carbon materials involves a solid-state process from an amorphous state to a crystalline state. According to the energy band model, the resistivity (ρ) of carbon materials is described by the following equation[47,48]:

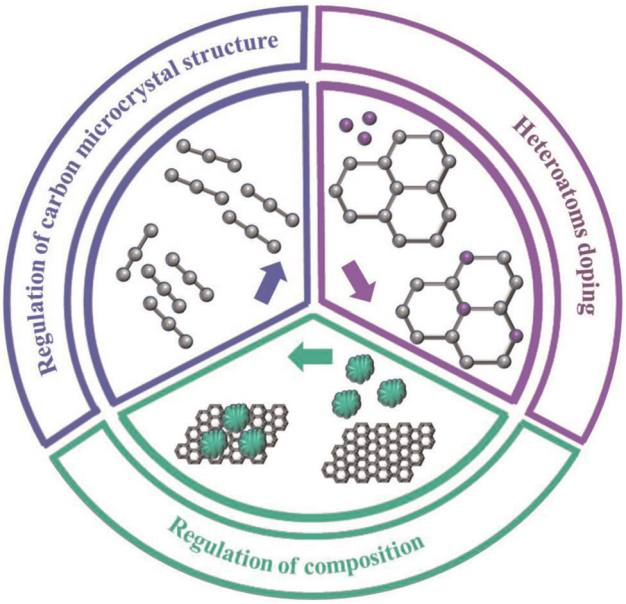

FIGURE 2 Design of framework to achieve high-rate KIBs

$$\rho = \frac{[\alpha(T) + \beta + \gamma(T)]}{r + e^{\left(\frac{\Delta E}{2KT}\right)}}, \tag{5}$$

where $\alpha(T)$ represents the term expressing the thermal lattice scattering effect, β represents the term expressing the boundary scattering effect, $\gamma(T)$ represents the term expressing the contact resistance, r represents free carrier concentration when $T = 0$ K, ΔE represents the energy bandgap, and K is the Boltzmann constant.

It is known that σ and ρ follow Ohm's law:

$$\sigma = \frac{1}{\rho}. \tag{6}$$

Obviously, the improvement of σ mainly contributes to the decrease in ρ. From Equation (5), the main factors affecting ρ are β and the carrier concentration ($e^{\left(-\frac{\Delta E}{2KT}\right)}$) at room temperature. The decrease in ρ for carbon materials is achieved by the enhancement of graphitization degree for the reason that high graphitic crystalline structure usually exhibits low ΔE, which is beneficial to the realization of high $e^{\left(-\frac{\Delta E}{2KT}\right)}$. More specifically, the interlayer spacing for carbon material decreases with the improvement of graphitization degree, resulting in the reduction of ΔE. So $e^{\left(-\frac{\Delta E}{2KT}\right)}$ is improved, which leads to the reduction in ρ. Therefore, high graphitic crystalline structure usually exhibits low ΔE, which is helpful for high $e^{\left(-\frac{\Delta E}{2KT}\right)}$ to achieve low ρ. To better evaluate the graphitization degree of carbon materials, the crystallite size (L_α) which represents the size of the microcrystalline in the plane direction of the carbon six-ring network, can be calculated by:

$$L_\alpha = (2.4 \times 10^{-10})\lambda^4 \left(\frac{I_D}{I_G}\right)^{-1}, \tag{7}$$

where λ is the laser line wavelength, and I_D and I_G are the integrated intensities of D and G Raman bands determined from Raman spectra, respectively.

Noticeably, the value of I_D/I_G determines the L_α, indicating that L_α increases with the enlargement of graphitization degree. What is noteworthy is that the enlargement of L_α also reduces β to achieve the decrease in ρ. Combining the above two factors, the conductivity of carbon materials increases with the enlargement of graphitization degree thanks to the increase in $e^{\left(-\frac{\Delta E}{2KT}\right)}$ and decrease in β.

High temperature treatment[49–51] and catalytic graphitization[52,53] are the two main methods to prepare carbon materials with high graphitic crystalline structure. Numerous research studies have confirmed that the higher graphitization degree of carbon materials can be obtained with a higher temperature. For example, three annealing temperatures (650°C, 1250°C, and 2800°C) were selected to prepare the carbon nanofibers with various microstructures (CNF-650, CNF-1250, and CNF-2800). The obtained CNF-650, CNF-1250, and CNF-2800 represented a disordered structure, partially ordered structure, and ordered structure, respectively, indicating that the graphitization degree was enlarged with increases in the annealing temperature (Figure 3A).[54] Due to the different graphitic crystalline structure, the three-carbon nanofibers showed different electronic conductivity as well as storage mechanism (Figure 3B), resulting in different rate performance in KIBs. Compared with CNF-650, a better electrochemical performance was obtained for CNF-1250 owing to the higher graphitization degree and a higher electronic conductivity (5.4 S cm^{-1}) than that of CNF-650 (10^{-4} S cm^{-1}). Although the electronic conductivity was further increased to 27.4 S cm^{-1} when elevating the temperature to 2800°C, CNF-2800 suffered a poor performance at the high current density due to the poor solid-state ion diffusivity in the graphitic structure with small layer spacing limiting the insertion of K^+.

Apart from high-temperature treatment, catalytic graphitization greatly reduces the graphitization temperature and shortens the graphitization time on the premise of the same graphitization degree as well. For instance, a graphitic nanocarbon with high graphitic crystalline structure was fabricated by the heat treatment of ethylenediaminetetraacetic acid nickel coordination compound and sodium chloride mixture at a low temperature of 600°C (Figure 3C,D).[55] The pyrolysis product of nickel metal inside the carbon skeleton served as a graphitization catalyst during the annealing process.

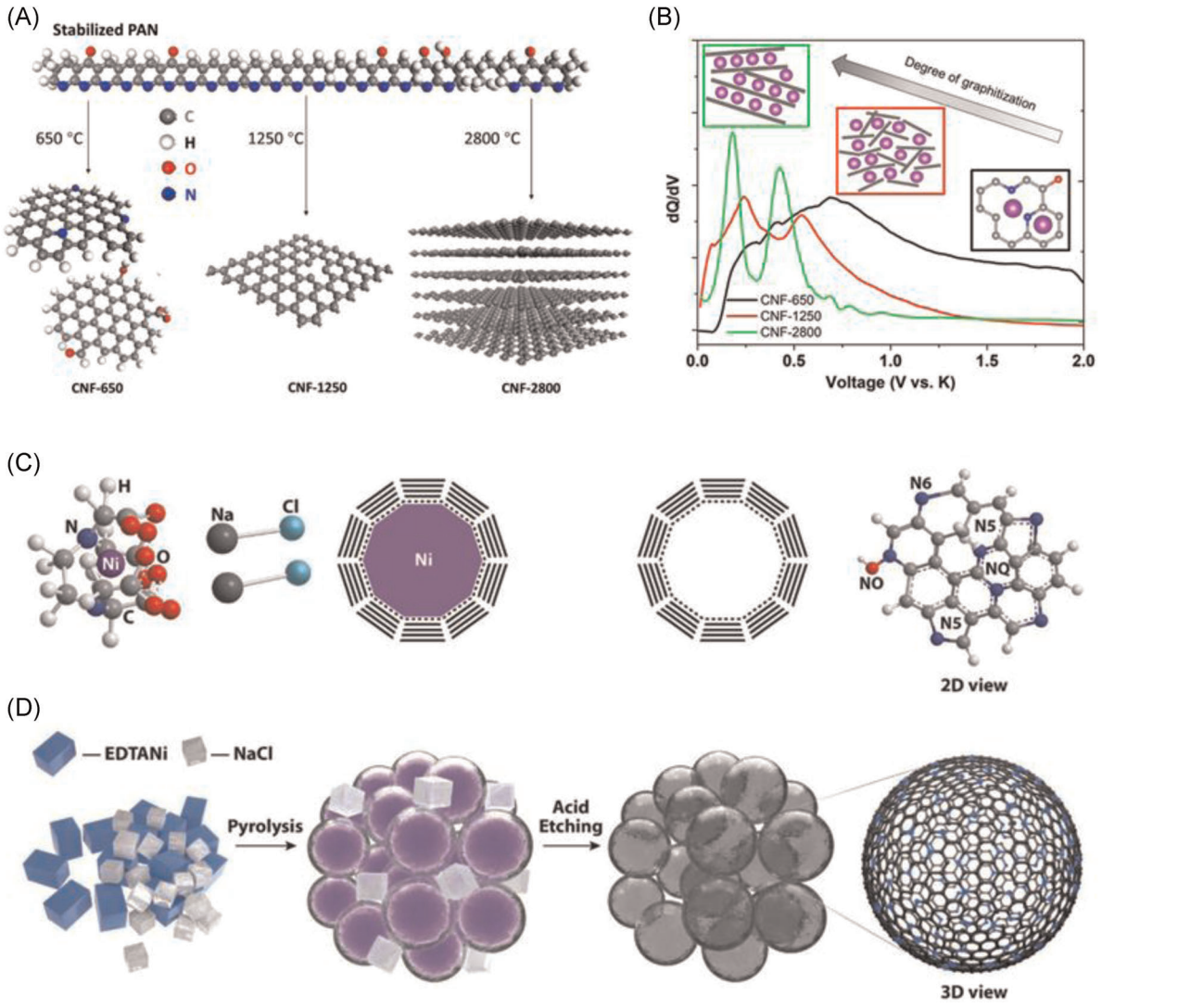

FIGURE 3 (A) Correlation between the microstructure of carbon nanofibers and the annealing temperature. (B) The dQ/dV curves of carbon nanofibers films at the oxidation. The inset shows the illustrations of the main K^+ storage mechanism in three different regions. Reproduced with permission: Copyright 2019, Elsevier.[54] (C,D) Schematic representation of the synthesis processes of graphitic nanocarbons. Reproduced with permission: Copyright 2019, Wiley[55]

With the assistance of facilitated graphitic structural features, the as-prepared anode sample exhibited attractive rate capability. The high capacity of 152 and 56.6 mAh g^{-1} were achieved at 1 and 5 A g^{-1}, respectively.

3.1.2 | Regulation of disordered structure

Carbon materials with high graphitic crystalline structure exhibit good electrical conductivity, but many of them usually suffer from poor kinetics problem in consequence of the narrow interlayer spacing and long diffusion distance. The narrow interlayer always results in a high ΔG, which hinders the facile intercalation of large-sized K^+. Moreover, the long diffusion distance slows down the K^+ diffusion rates within solid-state anode materials especially at high current densities. In this context, constructing disordered structure with expanded interlayer spacing is promising to solve the kinetics problem. Tai et al.[41] found that the ion diffusion coefficient of activated graphite with larger interlayer spaces was 7 times higher than that of graphite, thus enabling a better rate performance. An et al.[56] revealed that the electrochemical performance of commercial expanded graphite as anode material for KIBs was better than that of commercial graphite. Meanwhile, He et al.[57] reported that the hard carbon possessing a highly disordered structure delivered a considerable rate performance

(165.2 mAh g^{-1} at 4 A g^{-1}) when compared with the control sample possessing ordered structure (94.2 mAh g^{-1} at 4 A g^{-1}). These results clearly manifested that the larger interlayer spaces and disordered structure contributed to high-rate performance.

It is worth noting that although disordered structure boosts the K^+ diffusivity during charge/discharge process, the excessive degree of disorder may block the electronic conductions. In furtherance of rate capability, it is very essential to control the disorder degree reasonably to balance the electronic conductivity and ion diffusivity. Taking a multiwalled hierarchical carbon nanotube (HCNT) as an example, HCNT consisted of two clearly distinguished parts including an inner dense CNT with 4.5 nm wall thickness and outer loose CNT with 12.8 nm wall thickness (Figure 4A).[58] It was found that the inner CNT had straight and continuous walls that could serve as a robust skeleton to ensure fast electronic conduction; while the disordered structure in outer CNT ensures intensive reaction kinetics and high reaction efficiency of active material (Figure 4B). Thanks to the unique structure, HCNT displayed a satisfactory electrochemical performance such as a high capacity of 162 mAh g^{-1} at 1.6 A g^{-1}. Moreover, the disordered

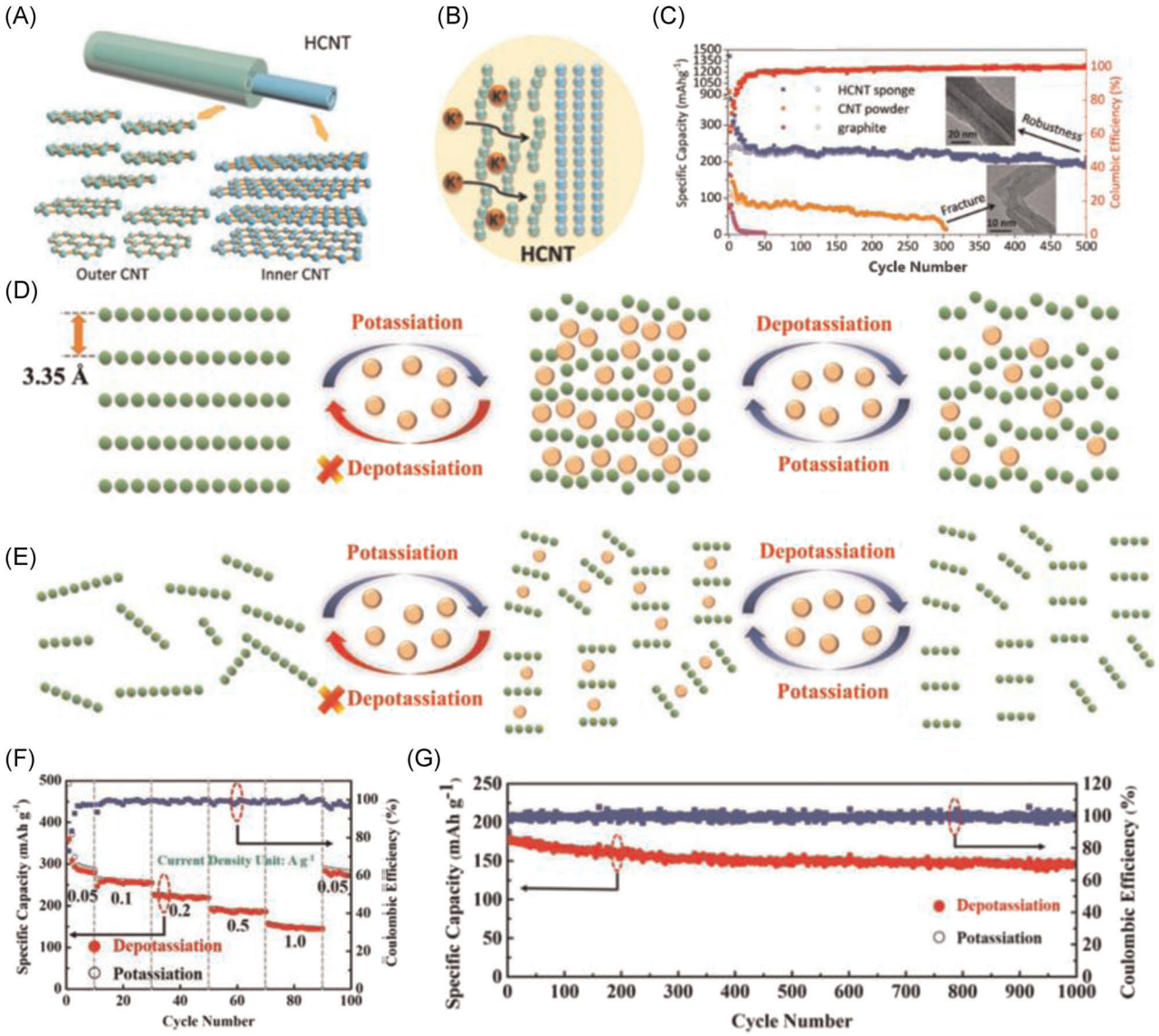

FIGURE 4 Schematic representation of (A) HCNT, (B) K^+ intercalation into HCNT walls. (C) Cycling performance of HCNT sponge anode, commercial CNT powder, and graphite anode at a current rate of 0.1 A g^{-1} for 500 cycles. Reproduced with permission: Copyright 2018, Wiley.[58] (D,E) Schematic representation of the potassiation and depotassiation process of graphite and OMC for KIBs. (F) Rate capability of OMC. (G) Long-term cycle stability and Coulombic efficiency at a high current density of 1 A g^{-1} over 1000 cycles. Reproduced with permission: Copyright 2018, Wiley[59]

structure with expanded interlayer spacing provided enough spaces to accommodate volume change to maintain structural stability. As shown in Figure 4C, HCNT delivered a high capacity of 232 mAh g^{-1} at 0.1 A g^{-1} with 90% retention after 500 cycles, while the capacity of commercial CNT powder and graphite powder decreased to zero after about 50 cycles and 300 cycles, respectively. Similarly, an amorphous ordered mesoporous carbon (OMC) possessing larger interlayer spacing in short range showed outstanding rate performance and cycling performance.[59] Figures 4D and 4E represent that the graphitic structure seriously collapsed during potassiation and depotassiation process, thus leading to the decrease of capacity. On the contrary, OMC maintained outstanding structural stability after continuous charging and discharging, and its large interlayer spacing and short diffusion distance ensured a higher diffusion coefficient of K^+, which led to excellent performance for OMC. As shown in Figure 4F, OMC delivered a capacity of 159.8 mAh g^{-1} at 1 A g^{-1} and maintained 146.5 mAh g^{-1} after 1000 cycles at 1 A g^{-1}, with an average capacity fading of 0.03% per cycle (Figure 4G).

Although a high graphitic structure has high electronic conductivity, the narrow interlayer spacing and long ion diffusion distance make it difficult for K^+ to intercalate into the carbon materials, thus resulting in poor ion diffusivity. A highly disordered structure can achieve good ion diffusivity but poor electronic conductivity due to the low graphitic crystalline structure. Therefore, rational regulation of carbon microcrystal structure is an effective way to balance the electronic conductivity and ion diffusivity of anode materials to achieve high-rate KIBs. However, optimizing a well-balanced graphitic crystalline structure and disordered structure in one carbon material remains a great challenge. Thus, further development of an efficient preparation strategy is an ongoing effort in the carbon field.

3.2 | Heteroatoms doping

Apart from the consideration of carbon framework microcrystal structure, heteroatoms doping (e.g., N, S, B) has been proven to be an effective way to propel the rate performance of anode materials by boosting both the electronic conductivity as well as ion diffusivity.[43,60,61] In general, dopants are divided into donor and acceptor according to the positive and negative charges they bring to the doped materials. Different heteroatom doping can be used as electron donors or acceptor to promote n-type conductivity and p-type conductivity respectively, which is favorable for the enhancement of electrochemical performance. For example, an S-doped reduced graphene oxide (S-RGO) sponge was prepared through heat treatment of graphene oxide sponge with S powder, which showed a lower polarization impedance compared with the reduced graphene oxide (RGO) before cycling as well as after 10 charge/discharge cycles, indicating that doped-S effectively promoted the electronic transport (Figure 5A–C).[61] Owing to the S doping, a specific capacity of 224 mAh g^{-1} at 1 A g^{-1} was realized for the S-RGO (Figure 5D). Moreover, N atoms are more easily doped into carbon materials compared with S atoms because N has the closest atomic radius to carbon, which brings great convenience to the doping of N atoms. It was found that the conductivity of N-doped carbon is obviously improved mainly because N atoms doped in carbon materials can be used as electron donors to promote n-type conductivity. More specifically, the electronic conductivity and rate of electron transfer are related to the apparent density of states at the Fermi level for semimetal carbonaceous materials.[63,64] In this context, N increases the lattice defects of graphite, resulting in an increase in the Fermi surface density of states and thus improving the conductivity of materials.[65,66] For example, Qi et al.[67] developed undoped carbon materials and N-doped carbon materials by the same synthesis method. It was found that the conductivity of N-doped carbon materials was 3.2 times higher than that of undoped carbon materials, which endowed N-doped carbon materials with a better rate capacity.

Interestingly, N can be doped in different positions of carbon materials to form different kinds of N species, which play a different role in the enhancing rate performance of KIBs. For example, three annealing temperatures (i.e., 500°C, 700°C, and 900°C) were selected to generate three N-doped carbon nanofibers (i.e., NCF-500, NCF-700, and NCF-900), which exhibited different kinds of N species corresponding to different conductivities.[62] The N1s spectrum showed the existence of three N species, including pyridinic N (N-6, 398.6 eV), pyrrolic N (N-5, 399.8 eV), and quaternary N (N-Q, 401.0 eV). As shown in Figure 5E, N-Q was located inside the graphitic carbon plane and bonds with three sp^2 carbon atoms, which was conducive to the electroconductibility of the graphitic carbon due to the significant change in the electron-donor characteristic.[68,69] N-5 and N-6 which are located in the edges or defect sites of carbon planes, serve as an electrochemically active site for adsorbing K^+ via a surface-dominated capacitive behavior, thus improving the fast diffusion ability rather than improving electronic conductivity. Figure 5F presents that the content of N-5 and N-6 obviously decreased while that of N-Q gradually increased with the increase in annealing temperature. According to the electroconductivity test (Figure 5G), with an increase in the content of N-Q, the electronic

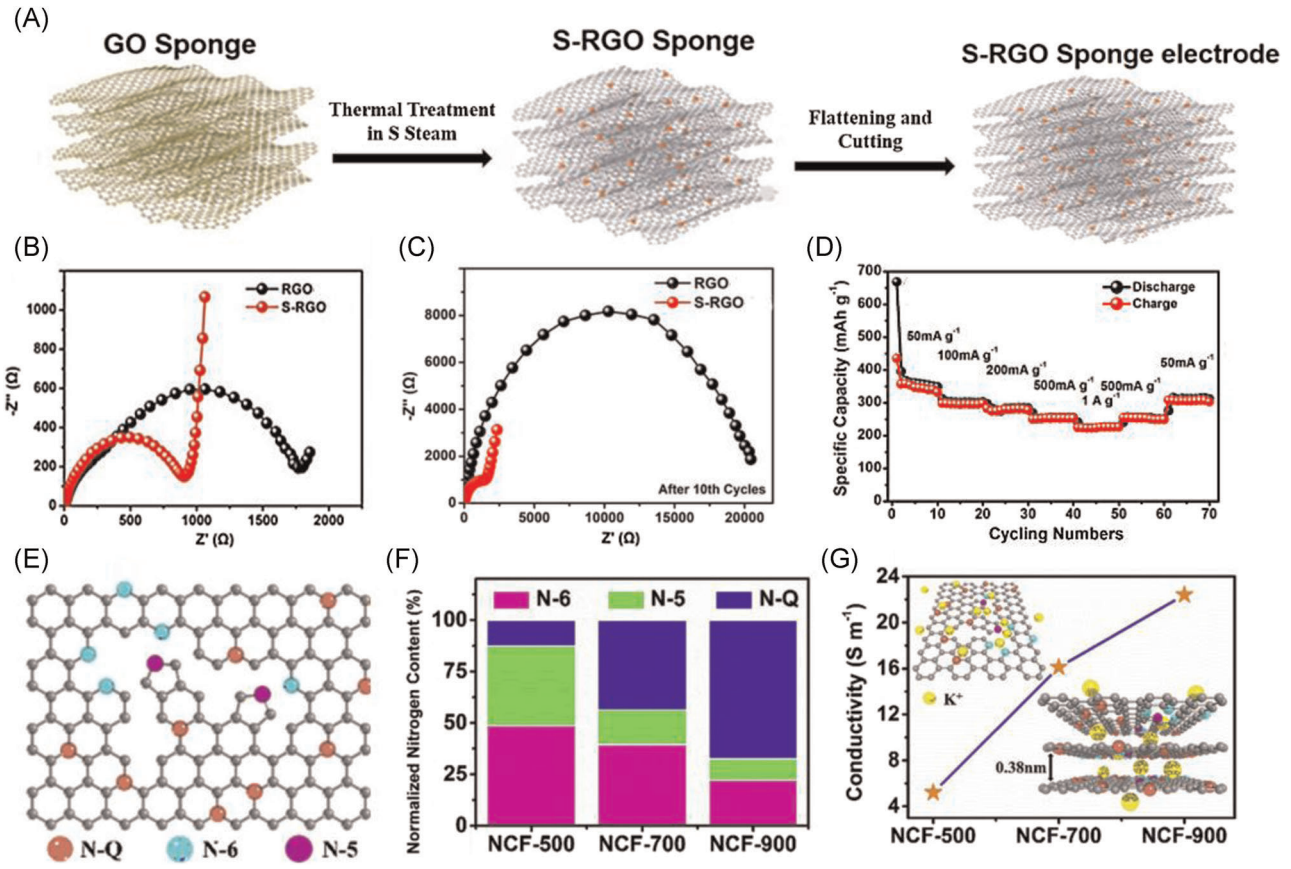

FIGURE 5 (A) Schematic representation of the synthesis process of S-RGO sponge electrode. (B,C) Electrochemical impedance spectra of RGO and S-RGO before and after 10 cycles, respectively. (D) Rate performance of S-RGO. Reproduced with permission: Copyright 2018, Elsevier.[61] (E) Location of N-Q, N-5, N-6, and (F) different content of N species in as-synthesized N-doped carbon nanofibers. (G) Electrical conductivity of the samples prepared at different temperatures. Inset: Illustration of K^+ adsorption and insertion behaviors. Reproduced with permission: Copyright 2018, Elsevier[62]

conductivity was significantly improved. The NCF-900 with more N-Q retained the electronic conductivity of 22.4 S cm^{-1}, which was higher than that of NCF-500 (5.2 S cm^{-1}) and NCF-700 (16.1 S cm^{-1}). This is because N-5 and N-6 located at the edge and defect can not increase the number of nonlocalized electrons, but N-Q which replaces carbon atom in graphite structures can introduce extra electrons. Depending on the superior electronic conductivity, a better rate performance than that of NCF-500 was obtained for NCF-900. However, it is worth noting that high-rate performance ascribes to not only the excellent electronic conductivity, but also the fast diffusion of K^+ driven by surface-controlled capacitive process. Thus, NCF-700 possessing high electronic conductivity and ion diffusivity showed the best performance.

Doping heteroatoms not only increases electronic conductivity, but also enhances ion diffusivity. For example, thanks to the doping of N atoms, N-doped porous carbon (NPC) represented a superior rate performance surpassing porous carbon because of the higher K^+ diffusion coefficient for NPC.[70] It was found that NPC delivered a capacity of 185 mAh g^{-1} at 10 A g^{-1}, while porous carbon without N doping only delivered a capacity of 82.5 mAh g^{-1} at the same current density. Figure 6A shows the potassium storage mechanism of NPC. K^+ could easily embed in NPC because N atoms expanded the layer spacing of the material, which effectively enhanced the diffusivity of K^+. Besides, doping heteroatoms into carbon materials not only generated a stronger attraction toward K^+ for its more electronegative than an undoped counterpart to promote ion diffusivity, but also created more active sites for K^+ storage to achieve good performance. Table 1 shows the comparison of the electrochemical properties of different doped carbon materials in KIBs. The N-doped carbons had enough active sites and larger layer spacing than the undoped counterparts.[82] When compared with N-Q, edge-N (N-5 and N-6) effectively changed the charge density distribution of carbon (Figure 6B–J), promoting K^+ adsorption and fast reaction kinetics.[71,73] However, the unreasonable distribution of edge-N and the neglect of N

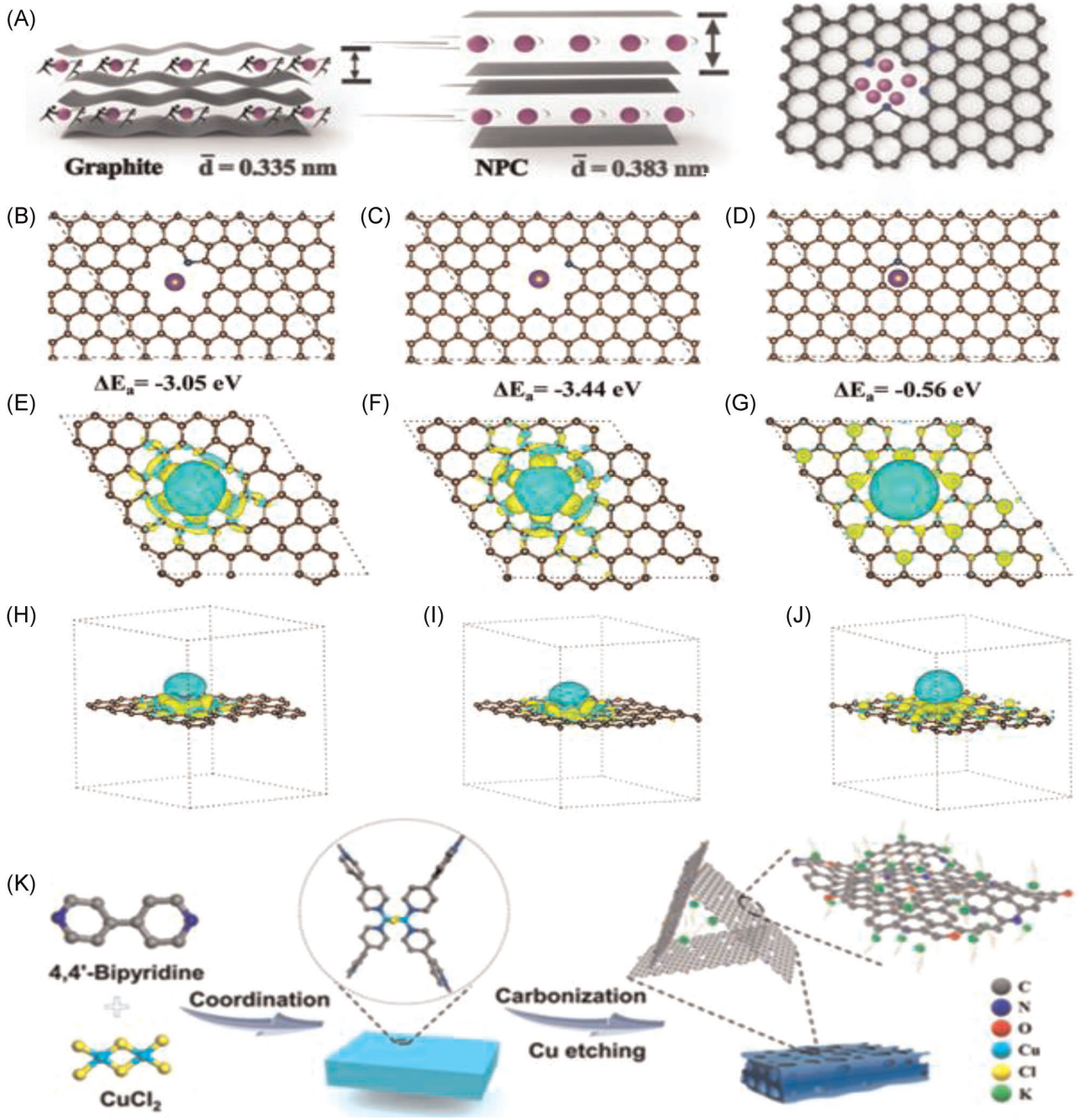

FIGURE 6 (A) Potassium storage mechanism of N-doped porous carbon. Reproduced with permission: Copyright 2018, Wiley.[70] K atom was absorbed in the (B) N-5, (C) N-6, and (D) N-Q-doped carbon structure. Side and top views of electron density differences of K absorbed in the (E,H) N-Q, (F,I) N-6, and (G,J) N-Q structures. Yellow and blue areas represent increased and decreased electron density, respectively. Brown, blue, and purple balls represent C, N, and K atoms, respectively. Reproduced with permission: Copyright 2019, Royal Society of Chemistry.[71] (K) Schematic representation of the synthesis of N-doped porous carbon nanosheets. Reproduced with permission: Copyright 2020, Wiley[72]

doping depth affected the performance of the batteries. Therefore, the design of carbon materials with edge-enriched N was of great significance to realize high-rate performance. For this reason, Xu et al.[72] proposed a low-temperature corrosion strategy based on pyridine coordination polymer (Figure 6K), in which aromatic pyridine was partially transferred to the edge-N heterocyclic carbon rings, and N doping and spatial distribution were reasonably controlled to obtain NPC nanosheets with high edge-N content of 9.34 at% and high surface area of 616 $m^2 g^{-1}$. The simultaneous realization of edge-N and high specific surface area was conducive to an

TABLE 1 Comparison of electrochemical performances of different doped carbon materials in potassium-ion batteries along with the heteroatom content and used electrolyte

Materials	Heteroatom content	Electrolyte	Rate capability	Cycle performance	References
NHC	N: 10.71 at%	0.8 M KPF_6 in EC:DEC = 1:1	2 A g^{-1}, 204.8 mAh g^{-1}	1 A g^{-1}, 1600 cycles, 161.3 mAh g^{-1}	[71]
NCNFs	N: 13.80 at%	0.8 M KPF_6 in EC:PC = 1:1	20 A g^{-1}, 101 mAh g^{-1}	2 A g^{-1}, 4000 cycles, 146 mAh g^{-1}	[73]
NPC	N: 6.88 at%	0.8 M KPF_6 in EC:DEC = 1:1	10 A g^{-1}, 185 mAh g^{-1}	5 A g^{-1}, 1000 cycles, 144.4 mAh g^{-1}	[70]
UNCN	N: 22.70 at%	0.8 M KPF_6 in EC:DMC:EMC = 4:3:2	6 A g^{-1}, 170 mAh g^{-1}	5 A g^{-1}, 3000 cycles, 110 mAh g^{-1}	[74]
ENDCs	N: 10.50 at%	0.8 M KPF_6 in EC:DEC = 1:1	5 A g^{-1}, 74 mAh g^{-1}	0.2 A g^{-1}, 660 cycles 305 mAh g–1	[75]
ENPCS	N: 11.80 at%	1.0 M KFSI in EMC	4 A g^{-1}, 110 mAh g^{-1}	1 A g^{-1}, 6000 cycles, 252 mAh g^{-1}	[72]
FFGF	F: 1.12 at%	0.8 M KPF_6 in EC:DEC = 1:1	0.5 A g^{-1}, 212.6 mAh g^{-1}	0.5 A g^{-1}, 200 cycles, 165.9 mAh g^{-1}	[43]
SNHC	N: 4.16 wt% S: 1.81 wt%	1.0 M KPF_6 in EC:DEC = 1:1	1.5 A g^{-1}, 199 mAh g^{-1}	3 A g^{-1}, 1200 cycles, 144.9 mAh g^{-1}	[76]
NSC	N: 2.09 at% S: 3.76 at%	0.8 M KPF_6 in EC:DEC=1:1	5 A g^{-1}, 115 mAh g^{-1}	1 A g^{-1}, 1000 cycles, 178 mAh g^{-1}	[77]
NSG	N: 5.86 at% S: 2.06 at%	0.8 M KPF_6 in EC:DEC = 1:1	20 A g^{-1}, 91.4 mAh g^{-1}	5 A g^{-1}, 5000 cycles, 100 mAh g^{-1}	[78]
MCOs	N: 1.09 at% O: 6.55 at%	1.0 M KPF_6 in EC:DEC = 1:1	1 A g^{-1}, 110 mAh g^{-1}	2 A g^{-1}, 3000 cycles, 80 mAh g^{-1}	[79]
NOHC	N: 2.02 at% O: 15.56 at%	0.8 M KPF_6 in EC:DEC = 1:1	5 A g^{-1}, 178.9 mAh g^{-1}	1 A g^{-1}, 5000 cycles, 189.5 mAh g^{-1}	[80]
OFPCN	O: 1.29 at% F: 0.16 at%	0.8 M KFSI in EC:DEC = 1:1	20 A g^{-1}, 78 mAh g^{-1}	1 A g^{-1}, 2000 cycles, 218 mAh g^{-1}	[81]

Abbreviations: ENDC, edge-N doped carbon; ENPCS, enriched N-doped porous carbon nanosheet; FFGF, few-layer F-doped graphene foam; MCO, N/O co-doped mesoporous carbon octahedron; NCNF, N-doped carbon nanofiber; NHC, ultrahigh pyrrolic/pyridinic-N-doped necklace-like hollow carbon; NOHC, N/O dual-doped hard carbon; NPC, N-doped porous carbon; NSC, N/S dual-doped porous soft carbon nanosheet; NSG, N/S dual-doped graphitic hollow architecture; OFPCN, O/F dual-doped porous carbon nanopolyhedra; SNHC, S/N dual-doped hard carbon; UNCN, ultrahigh N-doped carbon nanosheet.

efficient capacitive process, resulting in fast K^+ diffusion kinetics and thus showing impressive high capacity and rate performance. In addition, Zhang et al.[74] realized precise control of edge-N doping in carbon materials via molecular-scale copolymer pyrolysis strategy, and obtained defect-rich edge-N-doped carbons with a high N-doping up to 10.5 at% (edge-N ratio for 87.6 at%). The optimized material displayed excellent rate performance (74 mAh g^{-1} at 5 A g^{-1}) and long cycle life (93.8% retention after 3 months). Density functional theory calculations showed that when F was doped into graphene, the C–F bond formed for F and carbon can change the hybrid state of carbon from sp^2 to sp^3, resulting in local deformation of the material and thus having high electrical conductivity and thermodynamic stability.[83] Ju et al.[43] obtained a few layers of F-doped graphene foam by pyrolyzing polyvinylidene fluoride. It was found that partially doped-F provided favorable binding sites for K^+ around residual F atoms and facilitated the rapid transport of ions.

The attempt of multiple-element doping provides a new idea for the development of carbon anode materials. For example, compared with N doping, S/N co-doping further expanded interlayer spacing, and played a synergistic role in promoting electrochemical performance, which effectively enhanced K^+ ions adsorption and transportation.[78] By adjusting the number of heteroatoms (N and S), the layer spacing and edge defect degree of the

material can be effectively controlled to further promote the rapid transportation of ions. When it came to O and F doping, multiple K atoms could be adsorbed, and the O-/F-doped material exhibited ultrafast potassium storage performance.[81] In addition, although doping O into the carbon framework provided more active sites to heighten the capacity, it reduced the conductivity and led to poor cycle performance.[84] To cope with this drawback, dual-heteroatom doping (N and O) was designed and exhibited excellent cycling performance.[68]

Although a large number of heteroatom doping strategies have been reported, there is still less research on the realization of controllable doping positions and doping depths of heteroatoms. Meanwhile, for multiple element-doped carbon materials, the synergistic mechanism between elements needs to be further studied, and the relationship between doping and rapid charging and discharging of battery needs to be further investigated as well.

3.3 | Regulation of composition

Carbon materials generally have excellent electrical conductivity, but their low theoretical specific capacity may limit the batteries performance. Many noncarbon materials have high theoretical specific capacity but suffer from the rapid attenuation of batteries capacity due to the serious volume variation and/or poor electrical conductivity. Therefore, carbon/noncarbon composites come into spotlight because they can fully combine the advantages of carbon materials' high stability and electronic conductive, and noncarbon materials' high specific capacity. For example, Sb/carbon composite has been widely reported as anode materials for high-rate KIBs.[85–88] Wang et al.[86] synthesized an Sb/C composite that Sb nanoparticle completely embedded in porous carbon, which delivered a capacity of 200 mAh g^{-1} at 2 A g^{-1}. Similarly, a high capacity of 127 mAh g^{-1} at 2 A g^{-1} for Sb@graphene@carbon was achieved by Liu et al.[89]

Apart from Sb, many other metals were also introduced into the carbon materials to synthesize carbon-based composite. For instance, a carbon/Sn composite was obtained by the heat treatment of the polymer–Sn complex, demonstrating a high reversible capacity KIBs.[90] Yu et al.[91] synthesized carbon/Bi composite (Bi@3DGFs), in which Bi nanospheres were embedded in porous graphene frameworks (Figure 7A). Due to the unique structure, direct exposure of Bi to the electrolyte was prohibited, thus improving the interface stability of Bi.[93] Meanwhile, Bi not only heightened the specific capacity of the material, but also reduced the electrons' diffusion length, leading to high-rate performance. As shown in Figure 7B, the capacity of 154 and 113 mAh g^{-1} for Bi@3DGFs were obtained at the high current density of 5 and 10 A g^{-1}, respectively. Furthermore, the as-prepared composite retained a high reversible capacity of 164 mAh g^{-1} at 1 A g^{-1} after 400 cycles because the incorporation of carbon materials helped to buffer the volume expansion caused by the insertion of K^+ (Figure 7C).

Besides the alloying metals, some metal compounds also possess a high theoretical capacity and electronic conductivity due to their special structure, such as transition metal selenides. More importantly, their narrow bandgap semiconductor characteristic and sandwich structure made up of stacked atom layers endow them with high conductivity and fast ionic diffusion, which make them a promising candidate for KIBs. For example, $MoSe_2$ shows a large interlayer distance of 0.65 nm and remarkable electronic conductivity of 1×10^{-3} S m^{-1} due to the small bandgap of 1.1 eV. Shen et al.[94] prepared $MoSe_2$/C composite in which $MoSe_2$ on the surface of carbon not only promoted electronic conductivity, but also enabled combination with K^+ quickly, thus shortening the diffusion distance of K^+ to improve its diffusivity. Interestingly, the electrical conductivity of $MoSe_2$ was remarkably enhanced after the intercalation of potassium into $MoSe_2$.[95] Profited from these advantages, $MoSe_2$/C composite exhibited impressive rate performances such as a high capacity of 158 mAh g^{-1} even at a high rate of 2 A g^{-1}.

Another typical example is $CoSe_2$. The bandgap of $CoSe_2$ is zero, implying its excellent conductor property that is valuable for achieving high-rate performance. For instance, a metallic octahedral $CoSe_2$ threaded by CNTs ($CoSe_2$/C) showed a capacity of 196 mAh g^{-1} at a high current density of 2 A g^{-1}.[92] Furthermore, a long-time charge/discharge process was achieved, that is, a reversible capacity of 173 mAh g^{-1} at 2 A g^{-1} over 600 cycles with a capacity fading of only 0.03% per cycles (Figure 7F). The excellent rate performances were supposed to result from the unique structure. As shown in Figure 7D, $CoSe_2$/C presented a layered structure that every octahedral $CoSe_2$ particle arranged along the CNTs in sequence, leaving zigzag void space among particles. The CNTs not only served as a conductive network, but also accommodated the volume expansion to achieve long-term cycling stability. Simultaneously, $CoSe_2$ shows metallic property because of its zero bandgap structure, which suggests that the electrons can easily transfer to each $CoSe_2$ particle from the external circuit or in an opposite direction. As a consequence, the electrons can move quickly in the material, and K^+ effectively combined with $CoSe_2$ to shorten the diffusion time, thus realizing the high-rate K^+ storage (Figure 7E).

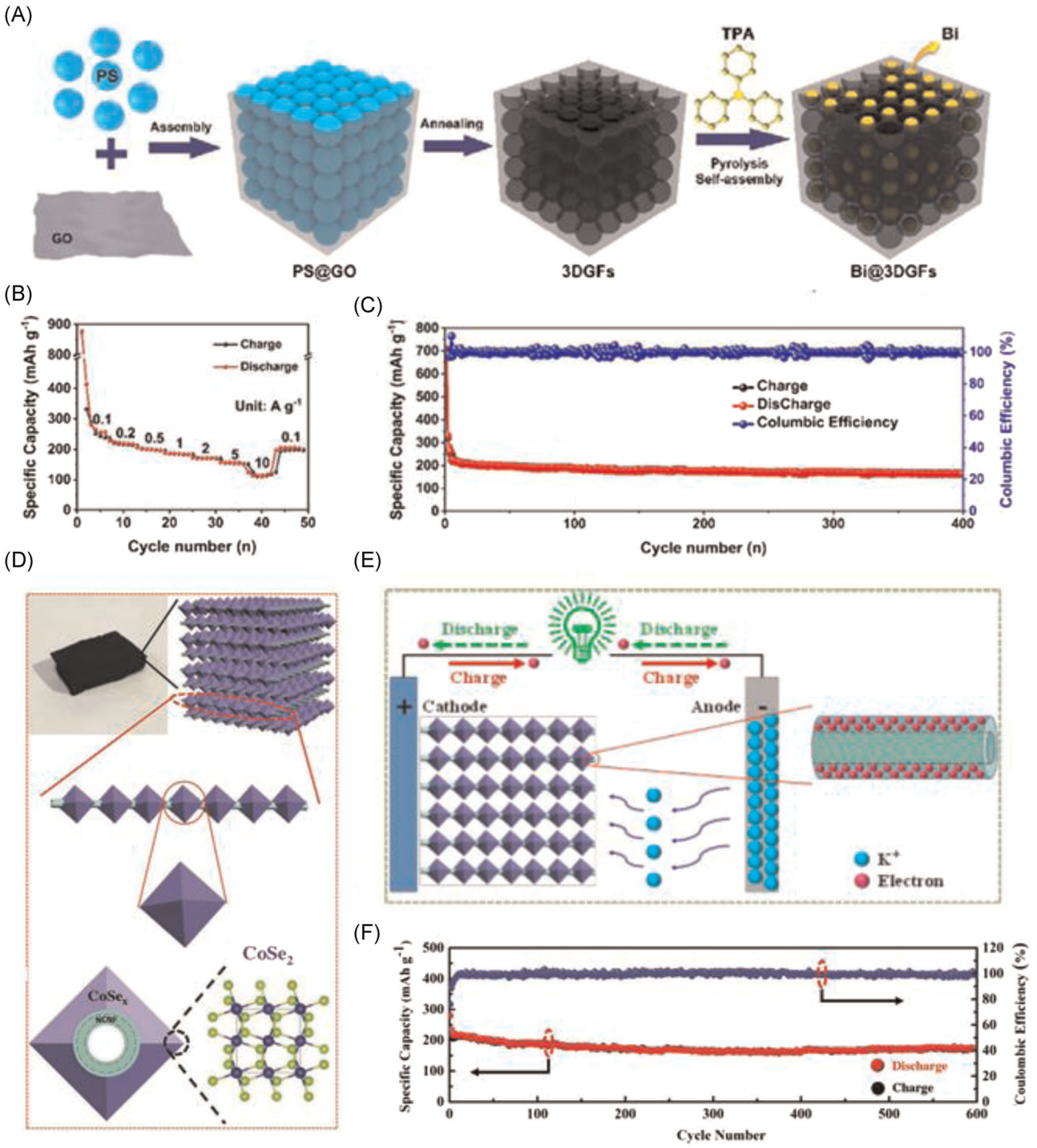

FIGURE 7 (A) Schematic representation of the synthesis procedure for Bi@3DGFs. (B) Rate capability of Bi@3DGFs anode. (C) Long cycle performance of Bi@3DGFs anode at 1 A g^{-1}. Reproduced with permission: Copyright 2019, Royal Society of Chemistry.[91] (D) Schematic representation of $CoSe_2$/C. (E) Schematic representation showing the electrochemical behavior in $CoSe_2$/C host. (F) Long-term cycling stability and Coulombic efficiency at a high current density of 2 A g^{-1} over 600 cycles of $CoSe_2$/C anode. Reproduced with permission: Copyright 2018, Wiley[92]

In addition to metal selenides/carbon composite, a large number of other carbon-based composites have also been proposed as the anode in KIBs, such as metal sulfides/carbon composite (e.g., CoS/C,[96] FeS_2/C,[97–99] MoS_2/C,[100] ReS_2/C,[101] SnS_2/C,[102] and MoS_2/SnO_2/C[103]), metal phosphide/carbon composite (e.g., CoP/C,[104] SnP_3/C,[105] and FeP/C[106]), metal oxide/carbon composite (e.g.,Fe_xO/C,[107] MoO_2/C,[108] SnO_2/C,[109] V_2O_3/C,[110] and Co_3O_4/

Fe_2O_3/C[111]) and metal nitride/carbon such as VN/C,[112] and showed remarkable potential in high-rate KIBs. Although carbon in these composites serves as a confining buffer to promote structural stability and enhance the electrical conductivity, more attention should be paid to well disperse active particles with a downsized size as much as possible into the carbon matrix, evenly to achieve the minimum volume expansion and high exposed active site for both long-term stability and high capacity. Besides, a deeper understanding of the respective working mechanisms should be explored so as to gain the appropriate materials which are widely used in KIBs. Especially, the low initial Coulombic efficiency resulting in large irreversible capacity loss,[113–115] and the high average potential with sloping curve affecting energy output in batteries would be the great challenges. It should be also noted that to realize the commercial application of these carbon-based composites in KIBs, some intrinsic limitations such as high-cost and low-yield synthetic technique should be circumvented in the future.

4 | DESIGN OF MORPHOLOGY

During the discharging process, K^+ depotassiates from the carbon anode and diffuses through the anode/electrolyte interface to the electrolyte. However, it is difficult for K^+ to diffuse from the interior of carbon materials to electrolyte quickly at high current densities because of the long diffusion distance. Considering the large size of K^+, strategies have focused on designing nanostructure and porous structure because they can improve the K^+ diffusivity/reaction kinetics by shortening the diffusion distance, thus enhancing rate capability.

Nanostructured carbon materials have the following advantages compared with traditional bulk materials.[116] (1) Nanostructured carbon materials can shorten the diffusion time of electrons and ions due to their lower dimensions. (2) Low dimensions and high specific surface area not only boost the contact area between carbon materials and electrolytes to promote the diffusivity, but also form the strong adhesion between the current collector and anode materials. (3) High surface energy and surface chemistry are favorable for nanostructured carbon materials to attract K^+.[117] (4) The distribution of various chemical bonding (sp^2, sp^3) gives nanostructured carbon materials better mechanical and chemical properties.

Additionally, it is known that abundant pores in favor of shortening the ionic diffusion distance improve the performance of KIBs. What is interesting is that the pores with different sizes have different functions, among which micropores (<2 nm) provide active site of ions storage, mesopores (2–50 nm) provide rich channels for the ion diffusion to reduce the resistance of ions transmission, and large pores (>50 nm) promote electrolyte penetration into the material to reduce the ionic diffusion distance.[118]

Consequently, nanostructured carbon materials with porous structure as anode materials will be essential in facilitating the electrochemical performance of KIBs. Table 2 shows the electrochemical performance of carbon-based anode with different morphologies in KIBs. Obviously, the rate performance was enhanced for the adjustment of ion diffusivity by constructing different dimensional and porous structures. In the following section, we will introduce some representative examples of the multiple-dimensional nanostructured porous carbon materials towards high-rate KIBs (Figure 8).

4.1 | Construction of zero-dimensional (0D) nanostructure

0D nanostructured carbon materials refer to the materials that have a spherical morphology with isotropic properties and the size all in nanoscale, indicating the electrons and ions have the shortest diffusion distances in all directions. As a result, 0D structure provides evident advantage in facilitating rate performance. There are two common structural designs for 0D carbon materials. The first one is the direct design of solid carbon nanospheres. For example, Gan et al.[128] synthesized the ultrafine solid carbon nanospheres with the size of about 20 nm, which delivered a high capacity of 157 mAh g^{-1} at an ultrahigh rate of 5 A g^{-1}. Moreover, the rate performance can be improved by changing the nanosize of carbon spheres. For instance, the nanosized and porous carbon spheres (SPCS) with diameters of 152 nm exhibited a better rate performance in KIBs compared with the nanosized carbon spheres (SCS) and carbon spheres (CS) corresponding diameters of 284 and 681 nm, respectively.[129] The different morphologies for these materials were ascribed to the synthetic method, in which tetraethyl orthosilicate was used to form pores and to further reduce the particle size (Figure 9A). By the agency of favorable structure for SPCS, it delivered a high capacity of 138.4 mAh g^{-1} at 2 A g^{-1}, while SCS and CS exhibited a low capacity of 111.6 and 51.2 mAh g^{-1} at the same current density, respectively (Figure 9B,C).

However, solid carbon nanospheres may suffer from the large volume expansion caused by the repeated potassiation/depotassiation of K^+, which will lead to poor electrochemical stability. For this reason, design of hollow carbon nanospheres becomes an attractive method to

TABLE 2 Electrochemical performances of the different dimensional carbonaceous anodes in potassium-ion batteries

Anode	Dimension	Ionic diffusivity ($cm^2 s^{-1}$)	Current density ($A g^{-1}$)	Capacity ($mAh g^{-1}$)	References
HCSs	0D	2.04×10^{-15}	2	~137.0	[119]
AHCSs	0D	6.85×10^{-15}	4	137.0	[119]
S/N@C	0D	1.44×10^{-12}	3.2	169.0	[120]
H–TiO_2–C	1D	7.32×10^{-14}	2	97.3	[121]
N–CNS	2D	8.15×10^{-9}	2	168.0	[122]
N–PCSs	3D	2.3×10^{-10}	5	185.0	[123]
NSC	3D	1.57×10^{-14}	2	151.6	[124]
NPC-600	3D	18.19×10^{-14}	2	186.2	[125]
PBPC-1000	3D	1.73×10^{-11}	1	152.0	[5]
ZSC@C@RGO	3D	1.88×10^{-17}	0.5	162.0	[126]
KTP@C	3D	8.84×10^{-12}	1	133.1	[127]
Sb@C	3D	1.12×10^{-10}	0.6	299.0	[88]
Sb@C-3DP	3D	4.99×10^{-10}	1	286.0	[88]

Abbreviations: AHCS, activated hollow carbon nanosphere; HCS, hollow carbon nanosphere; H–TiO_2–C, hierarchical tubular TiO_2–carbon heterostructure; KTP@C, hierarchical spheroid-like $KTi_2(PO_4)_3$@C; N–CNS, N-doped carbon nanosheet; NPC-600, N-doped porous carbon derived from ZIF-67 after carbonized at 600°C; N-PCS, N-doped porous carbon nanosheet; NSC, N/S co-doped carbon microboxes; PBPC-1000, potato-derived biomass porous carbon at 1000°C; S/N@C, S/N co-doped thin carbon; Sb@C, antimony–carbon composite; Sb@C-3DP, 3D microporous antimony–carbon composite; ZSC@C@RGO, tertiary hierarchical structure wrapped in reduced graphene oxide networks.

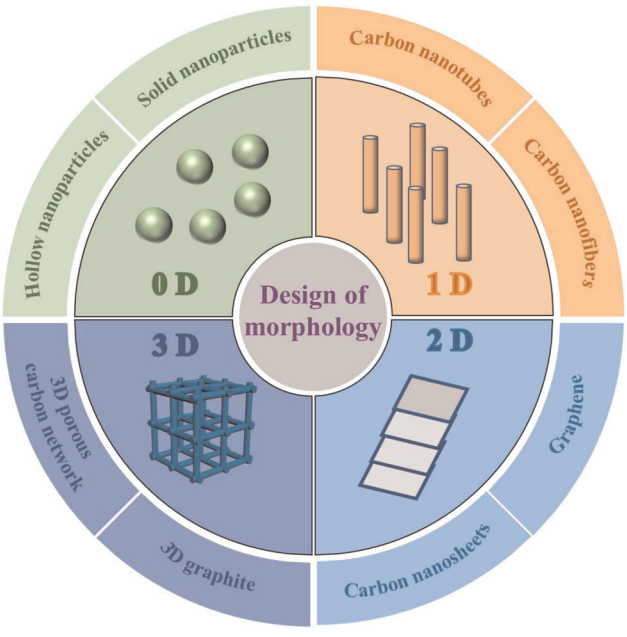

FIGURE 8 Carbon materials with different dimensionalities used in KIBs including zero-dimensional, one-dimensional, two-dimensional, and three-dimensional structure

promote the electrochemical performance,[119,120,129,131] because hollow carbon nanospheres can not only facilitate the stability of electrode materials for providing space for the volume expansion,[132] but also accelerate kinetics by shortening the ionic diffusion distance.[133,134] For example, Bin et al.[130] reported that the hollow carbon nanospheres showed a lower charge-transfer impedance and improved battery performance comparing with solid carbon nanospheres, indicating a hollow structure was in favor of fast metal ion transportation kinetics. Interestingly, the rate performance can be controlled by adjusting the shell number of hollow carbon nanospheres. As shown in Figure 9D, the authors used 3-aminophenol and formaldehyde solution as raw materials to synthesize the multishelled hollow carbon nanospheres (MS-HCNs) by carbonization. It was found that hollow carbon nanospheres with three shells showed the best rate performance and cycling performance in the shell-controlled series which possibly contributed to their mutual buffer effect and surface/interface metal-ion storage mechanism (Figure 9E).

Moreover, the internal cavity of hollow carbon nanospheres leaves great room for further control of their structure and optimization of their properties.[96] For example, the CoS/carbon core/shell nanocrystals that were

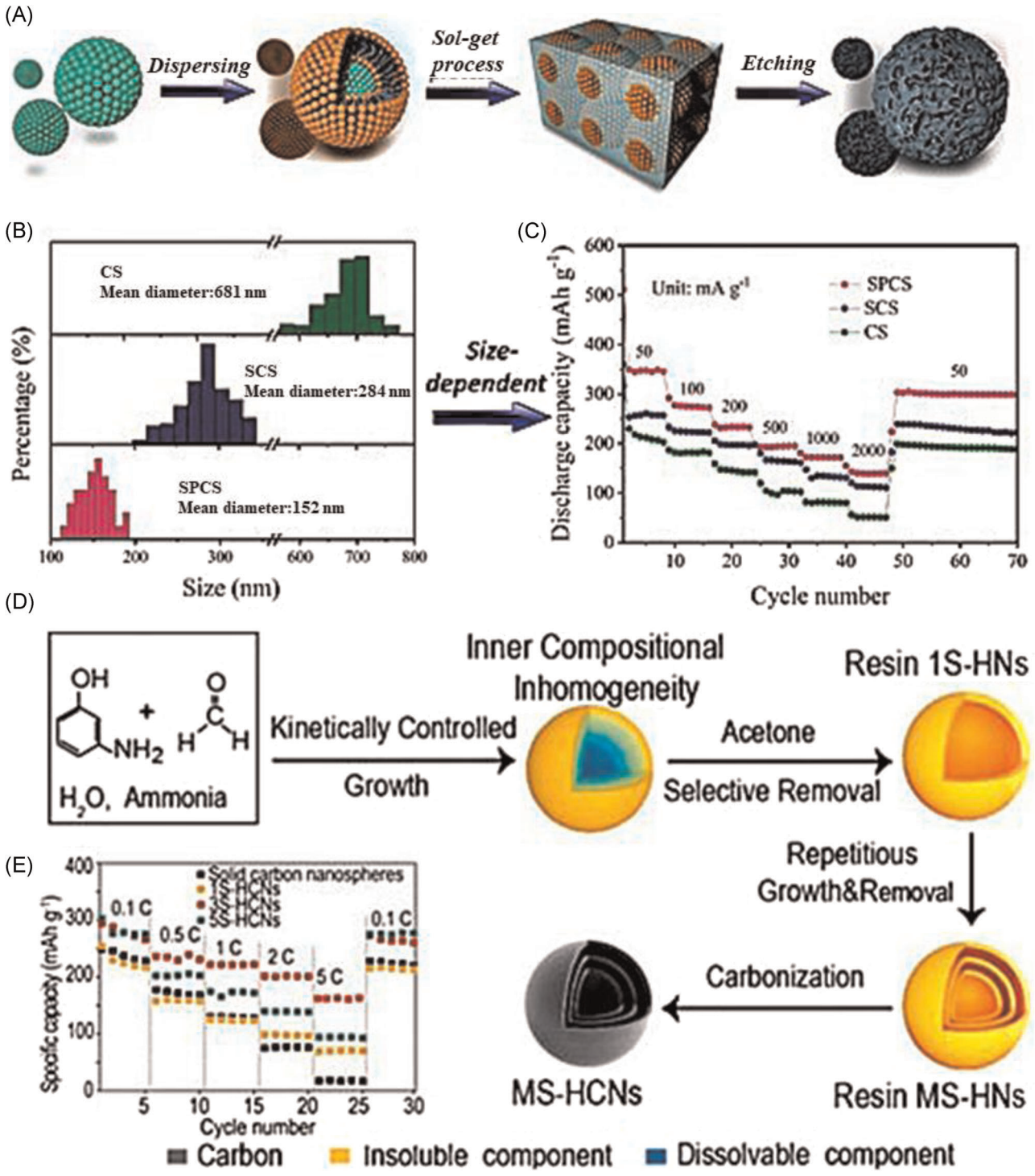

FIGURE 9 (A) Schematic representation of synthesizing SPCS. (B) Size distributions and (C) rate capability of CS, SCS, and SPCS. Reproduced with permission: Copyright 2020, Royal Society of Chemistry.[129] (D) Schematic representation of the synthesis of MS-HCNs via kinetically controlled growth. (E) Rate capabilities of solid carbon nanospheres and MS-HCNs. Reproduced with permission: Copyright 2017, American Chemical Society[130]

composed of 20–30 nm CoS core and amorphous carbon shell were reported by Yu et al.[96] The composite represented an admirable rate performance in KIBs. Likewise, yolk-shell carbon spheres (HYCS) were prepared through the extended Stöber reaction,[135] showing a better rate performance than that of solid carbon nanospheres because of the faster reaction kinetics and enhanced K^+ adsorption capability for HYCS (Figure 10A). Besides,

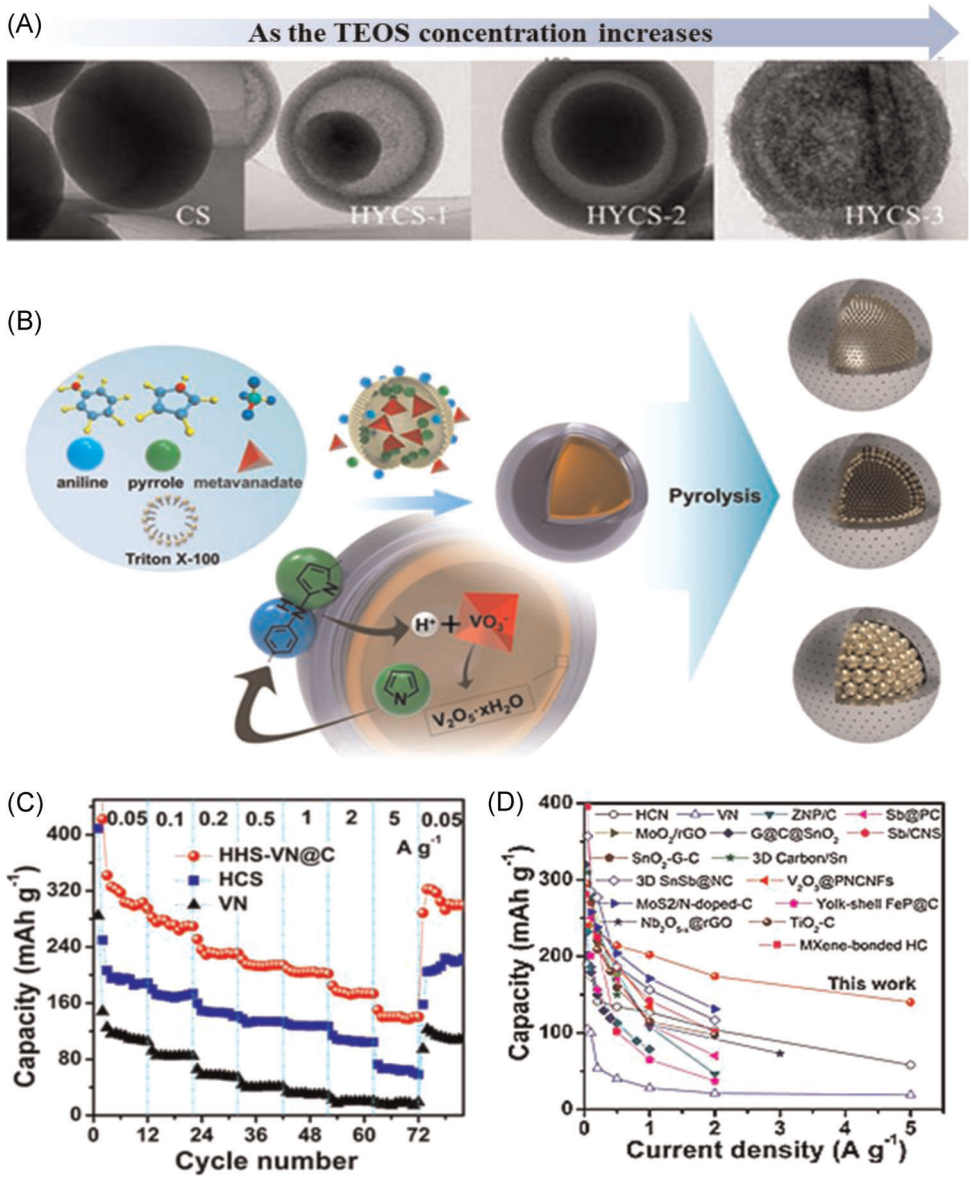

FIGURE 10 (A) Transmission electron microscopy images of solid carbon nanospheres and HYCS samples. Reproduced with permission: Copyright 2018, Royal Society of Chemistry.[135] (B) Schematic representation of the preparation of hollow hybrid spheres. (C) Rate performances for hollow hybrid spheres with an encapsulated VN nanocluster (HHS-VN@C), hollow carbon sphere (HCS), and VN. (D) Comparison of rate performances of reported carbon-based composites. Reproduced with permission: Copyright 2020, Elsevier[131]

different morphologies of HYCS can be well adjusted by controlling the tetraethyl orthosilicate concentration and the superior rate performance can be achieved.

Well dispersion of metallic compounds with ultrafine sizes encapsulated in hollow carbon spheres (HCSs) is of significance, and thus an exploration of a novel method to construct such architectures is still highly desirable and urgent. The current state-of-the-art synthetic methods are still problematic, because template-assisted selective etching or post-loading procedures suffer from tedious multistep procedures and high cost. And they show inadequate capability to rationally manipulate ultrafine nanoparticles (e.g., down to nanocluster) with adjustable content and compositional complexity, thus far restricting their potentials for highly efficient K^+ storage. Recently, Xu et al.[131] reported a versatile, general, and template-free synthesis of uniform hollow hybrid carbon nanospheres with various encapsulated ultrafine metal nitrides/oxides down to nanocluster scale, such as vanadium nitride (VN), vanadium oxide, molybdenum nitride, tungsten nitride, and bimetal-based nitrides. This was accomplished by one-pot aqueous solution chemistry with well-orchestrated

domino-driven reactions; the micelle-interfacial copolymerization was applied for the polymeric shell formation, and meanwhile, the copolymerization-generated H^+ spontaneously triggered oxometallate condensation inside micelles for encapsulation (Figure 10B). The proposed route simplifies the synthetic route by the integration of encapsulation and hollow shell formation in one pot without pre-existing templates, allowing the controlled loading of ultrafine nanoparticles. The unique combination of ultrafine encapsulated nanoparticles and hollow carbon architecture was demonstrated to promote the performances. Remarkable surface-dominated potassium storage with high capacity and high rate capability was shown using nanocluster VN in HCSs (Figure 10C). The performances exceed those of each single composition (hollow carbon and VN), and even the majority of previously reported materials so far, such as carbon composites with alloying metals, metal oxides/nitrides/sulfides, hard carbons, and graphitic carbons (Figure 10D), occupying a promising application prospect.

4.2 | Construction of one-dimensional (1D) nanostructure

1D nanostructured carbon materials (e.g., CNT and carbon nanofibers) can provide continuous electron transport pathways and short ionic diffusion distance to accelerate the electrons and ions transmission.[62,136] For example, Xiong et al.[137] prepared the CNTs with a hollow structure and an average outer diameter of ~20 nm. The CNTs aligned the graphene layers in a tilted angle with respect to their axis and featured an open structure on the surface, which led to the abundant exposed edges and facilitated the fast diffusion of K^+. It was demonstrated that such a 1D CNT delivered a high rate capability such as a high 102 mAh g^{-1} at 2 A g^{-1}. Shen et al.[1] synthesized the CNT encapsulated in sub-microcarbon fiber (SMCF@CNTs) via electrospinning and carbonizing with polyacrylonitrile and CNTs as precursors, in which the CNTs encapsulated in carbon fiber provided electronic transmission channel to achieve good battery performance (Figure 11A). As shown in Figure 11B,C, the SMCF@CNTs delivered an admired rate capacity (164 mAh g^{-1} at 5 C) and cycling performance (over 193 mAh g^{-1} after 300 cycles at 1 C).

In addition to CNTs, electrospun carbon nanofibers (CNFs) without the usage of conductive additives or binders were also widely studied as anode materials for KIBs because they enhanced the energy storage capability.[139,140] A far more appealing aspect of CNFs is that they can be used as flexible electrode materials due to their excellent mechanical strength. For this reason, CNFs have attracted great research interest in developing high-performance flexible batteries for wearable electronics.[141] For example, Adams et al.[142] used a CNF as flexible anode and demonstrated it showed a high capacity of 110 mAh g^{-1} at a very high rate of 10 C. Zhao et al.[143] also synthetized free-standing CNF with a good flexibility without rupture upon bending of 180°. The CNF anodes delivered a capacity of 140 mAh g^{-1} at 5 A g^{-1}. Even at 7.7 A g^{-1}, a capacity of 100 mAh g^{-1} was achieved. To further enhance the K^+ storage capability of CNF, Zhang et al.[138] used Sb@CNF composite as the anode materials of KIBs, in which Sb nanoparticles were finely encapsulated in mesoporous CNF. With these valuable fractures, the Sb significantly developed the capacities while the mesoporous CNF endowed high electronic conductivity and fast ion diffusivity with the resulting composites (Figure 11D). Consequently, the as-prepared Sb@CNF anode exhibited a high capacity of 161 mAh g^{-1} at 1 A g^{-1} and an ultralong cycling stability that retained a capacity of 130 mAh g^{-1} at 1 A g^{-1} after 1500 cycles.

4.3 | Construction of two-dimensional (2D) nanostructure

2D nanostructured carbon materials provide more abundant ion transport pathways when compared with 0D and 1D carbon materials, indicating the faster ionic diffusion rate for 2D carbon material. As a typical 2D carbon material, graphene was often used as the matrix material of carbon-based composites to achieve high-rate performance in KIBs.[108,144–146] For instance, a P@RGO composite with P particles embedded in RGO matrix can store K^+ up to a reversible capacity of 134.4 mAh g^{-1} at 2 A g^{-1}.[147] Moreover, a 2D G@porous FeS_2@C composite was developed to achieve a superior rate capacity of 298 mAh g^{-1} at 2 A g^{-1}, in which FeS_2 particles distributed on RGO matrix followed with an additional carbon coating layer.[148]

In addition to graphene, other 2D carbon materials such as carbon nanosheets have also exhibited excellent performance. For example, Liu et al.[122] found that 2D carbon nanosheets (Figure 12A) delivered a higher ion diffusivity (8.15×10^{-9} cm^2 s^{-1}) compared with solid carbon sphere and HCS (Figure 12B). The carbon nanosheets showed a 2D morphology of wrinkled envelope-like structure which was conducive to a shorter diffusion distance for K^+. Thus, at a high discharge rate of 2 A g^{-1}, the carbon nanosheets retained a high specific capacity of 168 mAh g^{-1} (Figure 12C). Similarly, a high reversible capacity of 185 mAh g^{-1} at 5 A g^{-1} for carbon nanosheets was reported by Li et al.[123] Moreover, a core–shell-like

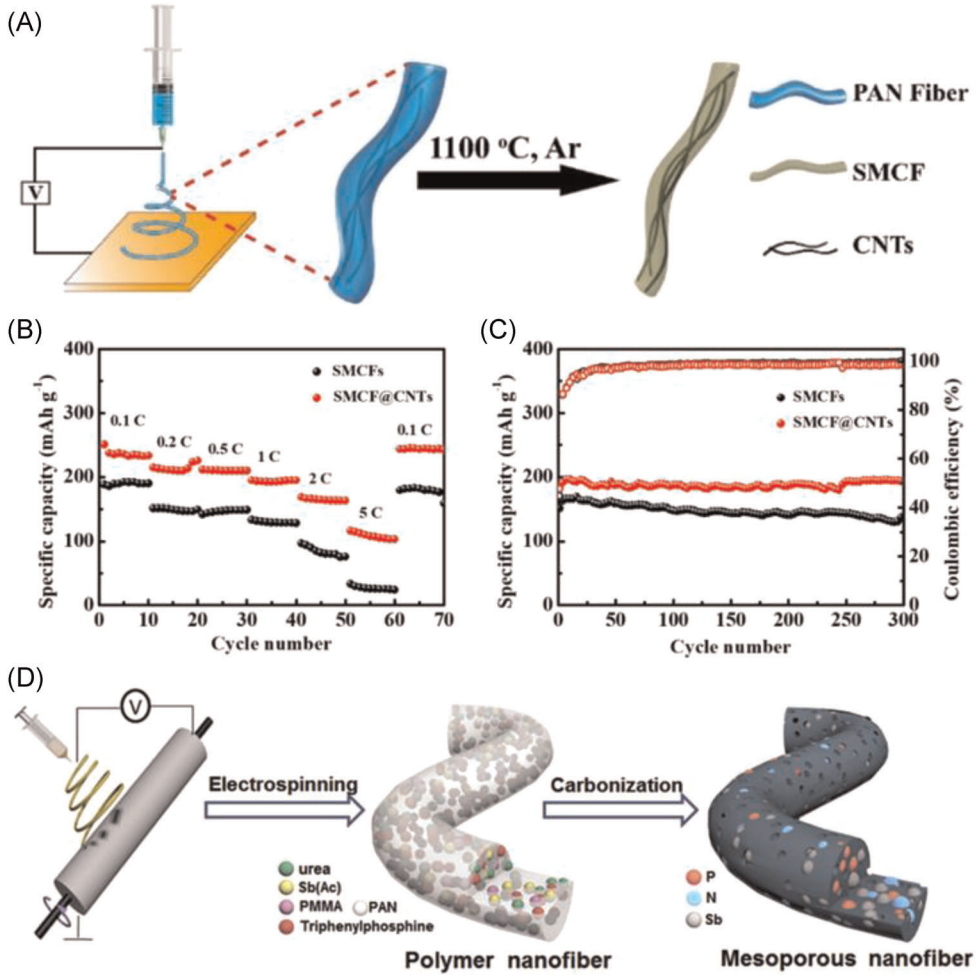

FIGURE 11 (A) Schematic representation for synthesizing SMCF@CNTs. (B) Rate performance of sub-microcarbon fibers and SMCF@CNTs. (C) Cycling performance of sub-microcarbon fibers and SMCF@CNTs at a current rate of 1 C. Reproduced with permission: Copyright 2019, American Chemical Society.[1] (D) Schematic representation of synthesizing Sb@CNF. Reproduced with permission: Copyright 2018, Elsevier[138]

cobalt phosphide nanoparticle embedded into carbon sheets with a 2D wrinkled structure had been synthesized (Figure 12D), in which the open space permitted easy permeation of the electrolyte and carbon sheets shortened the diffusion pathway of K^+, thereby showing favorable for electrochemical reactions.[104]

4.4 | Construction of three-dimensional (3D) nanostructure

3D electrodes offer great advantages for high-rate KIBs taking into account that they provide continuous transport pathways for both electrons and ions to enhance their transport kinetics. More importantly, 3D structure is instrumental in maintaining the mechanical stability effectively during high-rate cycling process. The fundamental understanding should be useful in the development of electrochemical performance in KIBs. Among various approaches, pyrolyzing metal–organic frameworks (MOFs) has been utilized to prepare 3D carbon materials by virtue of high surface area and mesopores which enhance the rate properties. For example, the mesoporous carbon octahedrons synthesized from pyrolysis of MOFs exhibited a high capacity of 110 mAh g^{-1} at 1 A g^{-1}.[79] Similarly, Li et al.[125] prepared a 3D porous carbon derived from the MOFs, and an outstanding rate capacity of 186.2 mAh g^{-1} at 2 A g^{-1} was obtained. It was found that mesopores provided enough channels for ionic diffusion, which was conducive to promoting the diffusivity of K^+, resulting in high-rate KIBs.

In addition, 3D hierarchical porous structure possesses multiple types of pores and usually displays the advantage of multimodal pores with a synergistic effect during the charging/discharging process. For example,

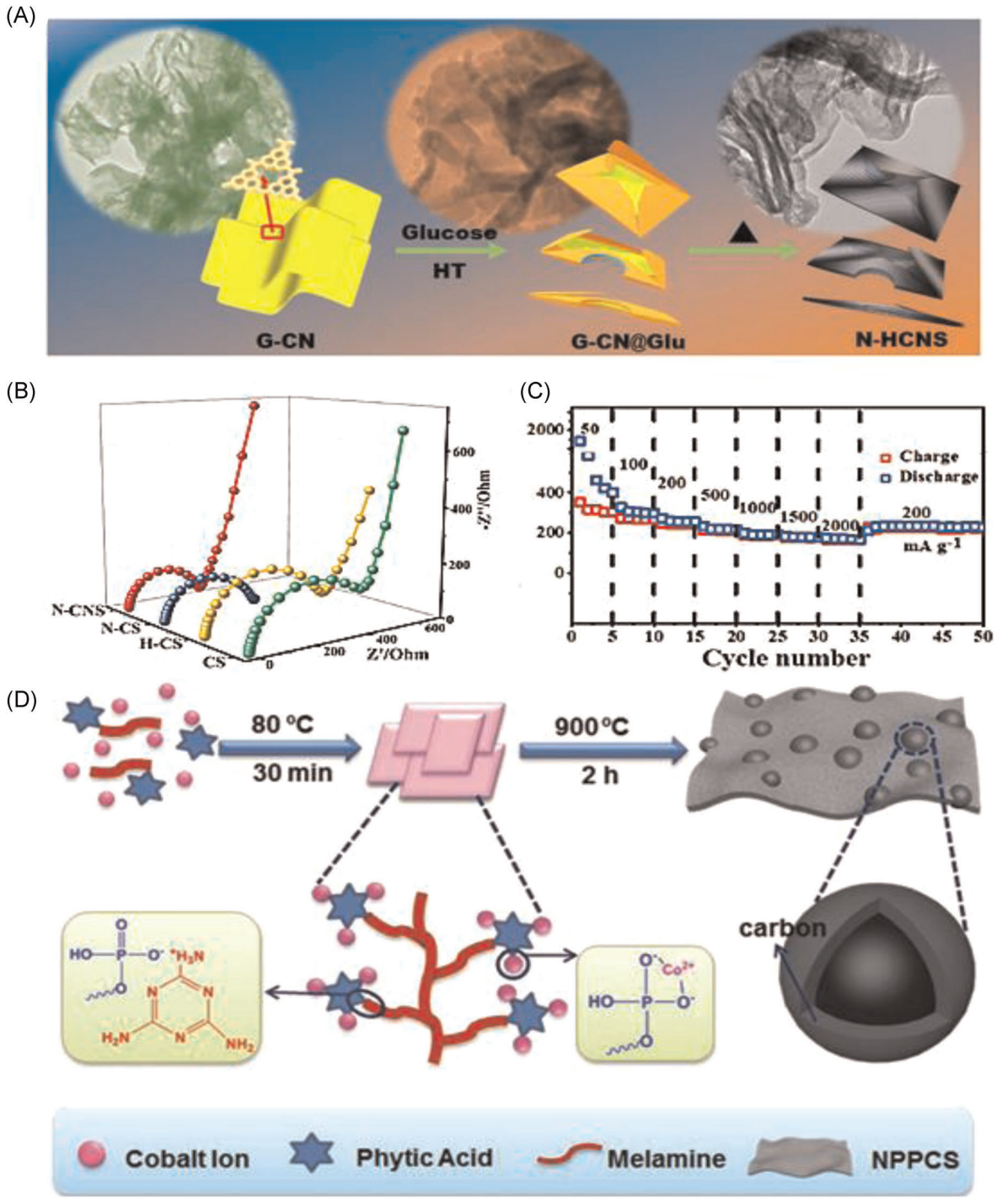

FIGURE 12 (A) Schematic representation of the fabrication of 2D carbon nanosheets. (B) Electrochemical impedance spectra of carbon sphere (CS), N-doped carbon sphere (N-CS), hollow carbon sphere (H-CS), and 2D N-doped carbon nanosheets (N-CNS). (C) Rate capability of N-CNS at different current densities. Reproduced with permission: Copyright 2018, Wiley.[122] (D) Schematic representation of synthesizing composite that core–shell-like cobalt phosphide nanoparticle embedded into carbon sheets. Reproduced with permission: Copyright 2018, Wiley[104]

the micropores inside the carbon framework can be used as active sites to increase the number of potassium storage sites. The mesopores and macropores promote the fast diffusion of K^+ to achieve high-rate performance. Recently, Zhang et al.[149] synthesized a 3D nanonetwork-structured carbon (NNSC) with a hierarchical porous structure (Figure 13B) and demonstrated that NNSC delivered a high-rate performance of KIB. As shown in

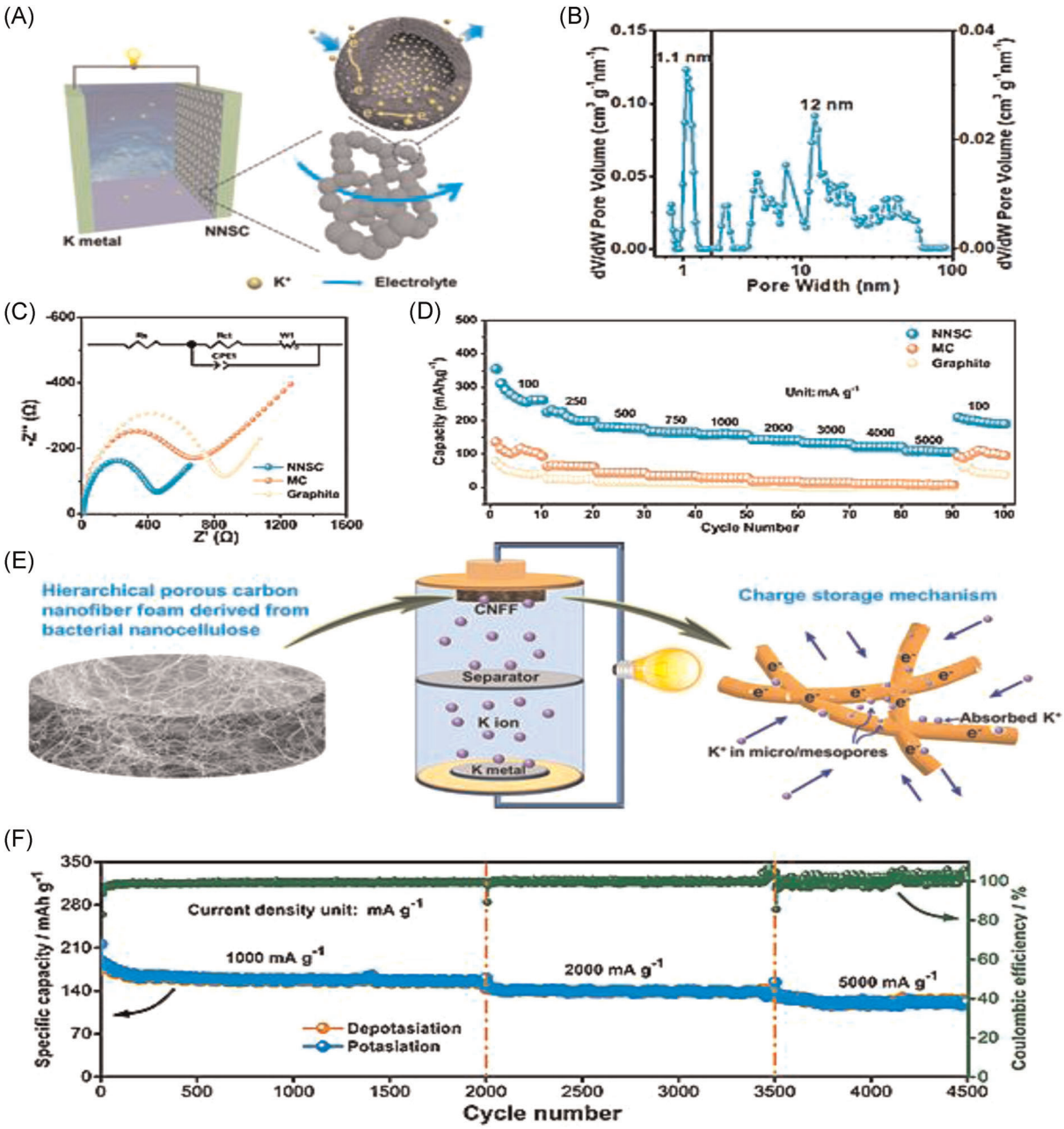

FIGURE 13 (A) Schematic representation of the reversible K^+ and electron transport process of NNSC anode. (B) Pore size distribution of NNSC. (C) Electrochemical impedance spectra of NNSC, MC, and graphite anodes. (D) Rate capability of NNSC, MC, and graphite anodes at current densities from 100 to 5 A g^{-1}. Reproduced with permission: Copyright 2020, Elsevier.[149] (E) Schematic representation of assembling carbon nanofiber foam freestanding anode into a potassium-ion battery. (F) Long-term cycling performances of carbon nanofiber foam anode at different current densities. Reproduced with permission: Copyright 2018, American Chemical Society[150]

Figure 13A, the tight connection between these nanospheres resulted in different degrees of agglomeration, thus forming a 3D conductive network and a hierarchical porous structure. Profited from the 3D hierarchical porous structure, the NNSC showed a lower charge-transfer resistance than that of microporous carbon (MC) and graphite, indicating faster K^+ diffusion rates for NNSC (Figure 13C). The calculated K^+ diffusion coefficient of the NNSC anode was 8.8 and 17.3 times higher than that of the MC and graphite anodes. As a result, NNSC showed a better rate performance with a high capacity of 108 mAh g^{-1} at 5 A g^{-1}, while MC and graphite suffered much inferior capacities at various current densities (Figure 13D). Additionally, Li et al.[150] reported a carbon

nanofiber foam with a 3D hierarchical porous structure (Figure 13E) and found that the carbon nanofiber showed an outstanding rate performance and a brilliant cycling performance. As shown in Figure 13F, the carbon nanofiber foam showed a capacity of 158 mAh g^{-1} at 1 A g^{-1} after 2000 cycles and the average lap loss was only 0.006%. After finishing the first 2000 cycles at 1 A g^{-1}, the electrode material remained at the capacities of 141 and 122 mAh g^{-1} at 2 A g^{-1} for 1500 cycles and 5 A g^{-1} for 1000 cycles, respectively. It was demonstrated that a 3D diffusion pathway supported by an electroconductive carbon network was responsible for the development in the capacity of this material.

Although nanostructured structure can facilitate the K^+ reaction kinetics to promote electrochemical performance, the low Coulombic efficiency and low packing density are still challenging when considering practical applications. Such low Coulombic efficiency will require excess of K-containing cathode to compensate for the irreversible loss of K, giving rise to low overall energy density. It is known that low Coulombic efficiency mainly originated from the severely irreversible side reactions or the undesirable surface reactions arising from the large surface area of nanomaterials and low electrochemical potential of K^+/K. To advance their applications in KIBs, several efficient ways could be used. (1) Well mixing nano- and micro-sized materials together in a certain proportion are beneficial to ensure the effective occupation of the space between the microparticles with nanosized particles. (2) Surface coating is demonstrated to be an effective way to mitigate the adverse surface reactions caused by large surface area of nanomaterials, thus improving the initial Coulombic efficiency.[151] (3) Development of hard–soft carbon composite is a common way to improve Coulombic efficiency.[152] (4) Exploration of novel electrolyte is necessary to make it compatible with carbon structure, thus improving reversible reactions.[153]

5 | CONCLUSIONS AND PROSPECTS

With the ever-increasing demand of LIBs, KIBs have been widely studied as alternative systems in recent years. At present, the high-rate charge/discharge capability is one of the main challenges to be addressed for the large-scale application of KIBs. To resolve this issue, the development of advanced anodes is of particular importance. A large number of carbonaceous materials with various structures/textures have been explored as anode materials for KIBs. Ingenious architecture engineering of carbonaceous anodes is demonstrated to be an efficient way to construct high-rate KIBs. Regulations of electronic conductivity and ion diffusivity of carbonaceous anodes are two key methods to realize high-rate performance, but a balance should be achieved between them. There are many techniques to control electronic conductivity and ion diffusivity of carbonaceous materials, among which the framework and morphology design of carbonaceous materials are the two most important strategies. In terms of framework design, tremendous efforts have been put to regulate carbon microcrystal structure, heteroatoms doping and composites with metallic compounds, which can affect ionic/electronic transport/reaction kinetics to varying degrees. Meanwhile, the morphology design of carbonaceous anodes can be realized by constructing nanostructures with different dimensions, and thus the ionic/electronic transport path and distance could be controlled to facilitate the rate performance as well.

Although a series of notable advancements have been acquired, there is still plentiful space for architecture science and engineering in the exploitation of advanced anodes for high-performance KIBs, especially for practical applications. A critical point is the low initial Coulombic efficiency, especially using the highly porous carbons. Such irreversible reactions will consume excess electrolyte and require higher cathode to anode capacity, leading to decreased overall energy density. In addition to Coulombic efficiency, other factors should be also taken into account from a practical viewpoint. (1) A long and stable plateau at low potential, rather than slope-dominated curve at high potential is required for carbon anodes, thus guaranteeing a high working voltage and high energy density in a full cell. (2) Carbon materials with high tap density is necessary to achieve high volumetric capacity and energy density. (3) The current mass loading is in the range of 1–2 mg cm^{-2}, and high mass loading of carbon anodes should be considered to achieve high areal capacity. (4) Carbon materials that are potentially scalable and inexpensive should be fabricated for low-cost energy storage.

Moreover, to surpass the existing battery vision, advanced characterization techniques, especially in situ operational technologies are highly necessary. Those advanced characterization technologies can track the evolution of the anode materials during the charging–discharging process and then determine the key influence factors, thus insightfully providing considerable inspiration for architecture design.

Additionally, it is very hard to realize high-rate KIBs only through developing advanced anode materials. Other constituents and parameters of KIBs (e.g., cathode, electrolyte, binder, separator, composition ratio, and fabrication technique of battery) are sensitive to the

electrochemical performances of the devices, and also need to be explored in depth.

ACKNOWLEDGMENTS

The authors gratefully acknowledge financial support from the projects of the National Natural Science Foundation of China (51972121, 51972270, 51702262), Tip-top Scientific and Technical Innovative Youth Talents of Guangdong Special Support Program (2017TQ04C419), Guangdong Province Universities and Colleges Pearl River Scholar Funded Scheme (2017), and Guangdong Basic and Applied Basic Research Foundation (2019A1515011502), the Natural Science Foundation of Shaanxi Province (2020JZ-07), and the Key Research and Development Program of Shaanxi Province (2019TSLGY07-03).

ORCID

Fei Xu https://orcid.org/0000-0003-2446-8903

REFERENCES

1. Shen C, Yuan K, Tian T, et al. Flexible sub-micro carbon fiber@CNTs as anodes for potassium-ion batteries. *ACS Appl Mater Interfaces*. 2019;11(5):5015-5021.
2. Marcus Y. Thermodynamic functions of transfer of single ions from water to nonaqueous and mixed solvents: Part I—Gibbs free energies of transfer to nonaqueous solvents. *Pure Appl Chem*. 1983;55(6):977-1021.
3. Han J, Xu M, Niu Y, et al. Exploration of $K_2Ti_8O_{17}$ as an anode material for potassium-ion batteries. *Chem Commun*. 2016;52(75):11274-11276.
4. Yabuuchi N, Kubota K, Dahbi M, Komaba S. Research development on sodium-ion batteries. *Chem Rev*. 2014;114(23):11636-11682.
5. Cao W, Zhang E, Wang J, et al. Potato derived biomass porous carbon as anode for potassium ion batteries. *Electrochim Acta*. 2019;293:364-370.
6. Jian ZL, Xing ZY, Bommier C, Li ZF, Ji XL. Hard carbon microspheres: potassium-ion anode versus sodium-ion anode. *Adv Energy Mater*. 2016;6(3):1501874.
7. Jian ZL, Luo W, Ji XL. Carbon electrodes for K-ion batteries. *J Am Chem Soc*. 2015;137(36):11566-11569.
8. Suo GQ, Li D, Feng L, Hou XJ, Yang YL, Wang WE. SnO_2 nanosheets grown on stainless steel mesh as a binder-free anode for potassium ion batteries. *J Electroanal Chem*. 2019;833:113-118.
9. Cao K, Liu H, Li W, et al. CuO nanoplates for high-performance potassium-ion batteries. *Small*. 2019;15(36):1901775.
10. Jiang HY, An YL, Tian Y, Feng JK, Tian XL. Scalable and controlled synthesis of 2D nanoporous Co_3O_4 from bulk alloy for potassium ion batteries. *Mater Technol*. 2020;35:1-6.
11. Li J, Rui B, Wei W, et al. Nanosheets assembled layered MoS_2/MXene as high performance anode materials for potassium ion batteries. *J Power Sources*. 2020;449:227481.
12. Sheng C, Zhang C, Shen X, et al. SnS_2/N-doped graphene as a superior stability anode for potassium-ion batteries by inhibiting "shuttle effect". *Batteries Supercaps*. 2020;3(1):56-59.
13. Yang L, Hong W, Tian Y, et al. Heteroatom-doped carbon inlaid with Sb_2X_3 (X = S, Se) nanodots for high-performance potassium-ion batteries. *Chem Eng J*. 2020;385:123838.
14. Miao W, Zhang Y, Li H, et al. ZIF-8/ZIF-67-derived 3D amorphous carbon-encapsulated CoS/NCNTs supported on CoS-coated carbon nanofibers as an advanced potassium-ion battery anode. *J Mater Chem A*. 2019;7(10):5504-5512.
15. Yu S, Kim SO, Kim HS, Choi W. Computational screening of anode materials for potassium-ion batteries. *Int J Energy Res*. 2019;43(13):7646-7654.
16. Zhang W, Wu Z, Zhang J, et al. Unraveling the effect of salt chemistry on long-durability high-phosphorus-concentration anode for potassium ion batteries. *Nano Energy*. 2018;53:967-974.
17. Zhang W, Pang WK, Sencadas V, Guo Z. Understanding high-energy-density Sn_4P_3 anodes for potassium-ion batteries. *Joule*. 2018;2(8):1534-1547.
18. Wang Q, Zhao X, Ni C, et al. Reaction and capacity-fading mechanisms of tin nanoparticles in potassium-ion batteries. *J Phys Chem C*. 2017;121(23):12652-12657.
19. Gabaudan V, Berthelot R, Stievano L, Monconduit L. Inside the alloy mechanism of Sb and Bi electrodes for K-ion batteries. *J Phys Chem C*. 2018;122(32):18266-18273.
20. Yang Q, Wang ZF, Xi W, He G. Tailoring nanoporous structures of Ge anodes for stable potassium-ion batteries. *Electrochem Commun*. 2019;101:68-72.
21. Lei K, Wang C, Liu L, et al. A porous network of bismuth used as the anode material for high-energy-density potassium-ion batteries. *Angew Chem Int Ed*. 2018;57(17):4687-4691.
22. Zhang Y, Li M, Huang F, et al. 3D porous Sb-Co nanocomposites as advanced anodes for sodium-ion batteries and potassium-ion batteries. *Appl Surf Sci*. 2020;499:143907.
23. Gabaudan V, Berthelot R, Sougrati MT, Lippens P-E, Monconduit L, Stievano L. SnSb vs. Sn: improving the performance of Sn-based anodes for K-ion batteries by synergetic alloying with Sb. *J Mater Chem A*. 2019;7(25):15262-15270.
24. Liang Y, Luo C, Wang F, et al. An organic anode for high temperature potassium-ion batteries. *Adv Energy Mater*. 2019;9(2):1802986.
25. Wang C, Tang W, Yao ZY, Chen YZ, Pei JF, Fan C. Using an organic acid as a universal anode for highly efficient Li-ion, Na-ion and K-ion batteries. *Org Electron*. 2018;62:536-541.
26. Deng Q, Pei J, Fan C, et al. Potassium salts of para-aromatic dicarboxylates as the highly efficient organic anodes for low-cost K-ion batteries. *Nano Energy*. 2017;33:350-355.
27. Li C, Deng Q, Tan H, et al. Para-conjugated dicarboxylates with extended aromatic skeletons as the highly advanced organic anodes for K-ion battery. *ACS Appl Mater Interfaces*. 2017;9(33):27414-27420.
28. Zhao Q, Wang JB, Lu Y, Li YX, Liang GX, Chen J. Oxocarbon salts for fast rechargeable batteries. *Angew Chem Int Ed*. 2016;55(40):12528-12532.
29. Naylor AJ, Carboni M, Valyo M, Younesi R. Interfacial reaction mechanisms on graphite anodes for K-ion batteries. *ACS Appl Mater Interfaces*. 2019;11(49):45636-45645.

30. Jo J, Lee S, Gim J, et al. Facile synthesis of reduced graphene oxide by modified hummer's method as anode material for Li-, Na- and K-ion secondary batteries. *Royal Soc Open Sci*. 2019;6(4):181978.
31. Peng ST, Wang LC, Zhu ZQ, Han K. Electrochemical performance of reduced graphene oxide/carbon nanotube hybrid papers as binder-free anodes for potassium-ion batteries. *J Phys Chem Solids*. 2020;138:109296.
32. Zhang Y, Tian S, Yang CH, Nan JM. Three-dimensional nitrogen-sulfur codoped layered porous carbon nanosheets with sulfur-regulated nitrogen content as a high-performance anode material for potassium-ion batteries. *Dalton Trans*. 2020;49(16):5108-5120.
33. Lei YH, Qin L, Zhai DY, Kang FY. Research progress on carbon anode materials in potassium-ion batteries. *New Carbon Mater*. 2019;34(6):499-511.
34. Gao XR, Zheng X, Li ZJ, Dong XY, Ju ZC, Guo CL. A review on recent advances in carbon aerogels: their preparation and use in alkali-metal ion batteries. *New Carbon Mater*. 2020; 35(5):486-507.
35. Wu XY, Leonard DP, Ji XL. Emerging non-aqueous potassium-ion batteries: challenges and opportunities. *Chem Mater*. 2017;29(12):5031-5042.
36. Zhu GL, Zhao CZ, Huang JQ, et al. Fast charging lithium batteries: recent progress and future prospects. *Small*. 2019; 15(15):1805389.
37. Sha M, Liu L, Zhao H, Lei Y. Anode materials for potassium-ion batteries: current status and prospects. *Carbon Energy*. 2020;2(3):350-369.
38. Carboni M, Naylor AJ, Valvo M, Younesi R. Unlocking high capacities of graphite anodes for potassium-ion batteries. *RSC Adv*. 2019;9(36):21070-21074.
39. Fan L, Ma RF, Zhang QF, Jia XX, Lu BG. Graphite anode for a potassium-ion battery with unprecedented performance. *Angew Chem Int Ed*. 2019;58(31):10500-10505.
40. He ZK, Sun Q, Xie KY, Lu P, Shi ZN, Kamali AR. Reactive molten salt synthesis of natural graphite flakes decorated with SnO_2 nanorods as high performance, low cost anode material for lithium ion batteries. *J Alloys Compd*. 2019;792:1213-1222.
41. Tai ZX, Zhang Q, Liu YJ, Liu HK, Dou SX. Activated carbon from the graphite with increased rate capability for the potassium ion battery. *Carbon*. 2017;123:54-61.
42. Fang L, Xu J, Sun S, et al. Few-layered tin sulfide nanosheets supported on reduced graphene oxide as a high-performance anode for potassium-ion batteries. *Small*. 2019;15(10): 1804806.
43. Ju Z, Zhang S, Xing Z, Zhuang QC, Qiang YH, Qian Y. Direct synthesis of few-layer F-doped graphene foam and its lithium/potassium storage properties. *ACS Appl Mater Interfaces*. 2016;8(32):20682-20690.
44. Zhao W, Shen Y, Zhang H, et al. Porous-carbon aerogels with tailored sub-nanopores for high cycling stability and rate capability potassium-ion battery anodes. *ACS Appl Mater Interfaces*. 2020;12(24):27045-27054.
45. Cheng N, Zhao J, Fan L, et al. Sb-MOFs derived Sb nanoparticles@porous carbon for high performance potassium-ion batteries anode. *Chem Commun*. 2019;55(83):12511-12514.
46. Du JC, Gao SS, Shi PH, Fan JC, Xu QJ, Min YL. Three-dimensional carbonaceous for potassium ion batteries anode to boost rate and cycle life performance. *J Power Sources*. 2020;451:227727.
47. Zhang FQ, Huang QZ, Huang BY, Gong QM, Chen TF. Effects of graphitization degree on the electrical conductivity of C/C composites. *New Carbon Mater*. 2001;16(2):45-48.
48. Yu L, Liu QF, Qiao ZC, Cui XJ, Yuan L. Study on the relationship between the microcrystalline structure of coal-based graphite and its electrical conductivity. *Carbon Tech*. 2017;36(5):14-18.
49. Kasahara N, Shiraishi S, Oya A. Heterogeneous graphitization of thin carbon fiber derived from phenol–formaldehyde resin. *Carbon*. 2003;41(8):1654-1656.
50. Inagaki M, Fujita K, Takeuchi Y, Oshida K, Konno H. Formation of graphite crystals at 1000–1200°C from mixtures of vinyl polymers with metal oxides. *Carbon*. 2001;39(6):921-929.
51. Fuertes AB, Alvarez S. Graphitic mesoporous carbons synthesised through mesostructured silica templates. *Carbon*. 2004;42(15):3049-3055.
52. Zhai D, Du H, Li B, Zhu Y, Kang F. Porous graphitic carbons prepared by combining chemical activation with catalytic graphitization. *Carbon*. 2011;49(2):725-729.
53. Maldonado-Hódar FJ, Moreno-Castilla C, Rivera-Utrilla J, Hanzawa Y, Yamada Y. Catalytic graphitization of carbon aerogels by transition metals. *Langmuir*. 2000;16(9): 4367-4373.
54. Lin XY, Huang JQ, Zhang B. Correlation between the microstructure of carbon materials and their potassium ion storage performance. *Carbon*. 2019;143:138-146.
55. Zhang W, Ming J, Zhao W, et al. Graphitic nanocarbon with engineered defects for high-performance potassium-ion battery anodes. *Adv Funct Mater*. 2019;29(35):1903641.
56. An Y, Fei H, Zeng G, et al. Commercial expanded graphite as a low cost, long-cycling life anode for potassium-ion batteries with conventional carbonate electrolyte. *J Power Sources*. 2018;378:66-72.
57. He X, Liao J, Tang Z, et al. Highly disordered hard carbon derived from skimmed cotton as a high-performance anode material for potassium-ion batteries. *J Power Sources*. 2018; 396:533-541.
58. Wang Y, Wang Z, Chen Y, et al. Hyperporous sponge interconnected by hierarchical carbon nanotubes as a high-performance potassium-ion battery anode. *Adv Mater*. 2018; 30(32):1802074.
59. Wang W, Zhou J, Wang Z, et al. Short-range order in mesoporous carbon boosts potassium-ion battery performance. *Adv Energy Mater*. 2018;8(5):1701648.
60. Chen C, Wang Z, Zhang B, et al. Nitrogen-rich hard carbon as a highly durable anode for high-power potassium-ion batteries. *Energy Stor Mater*. 2017;8:161-168.
61. Li J, Qin W, Xie J, et al. Sulphur-doped reduced graphene oxide sponges as high-performance free-standing anodes for K-ion storage. *Nano Energy*. 2018;53:415-424.
62. Hao R, Lan H, Kuang CW, Wang H, Guo L. Superior potassium storage in chitin-derived natural nitrogen-doped carbon nanofibers. *Carbon*. 2018;128:224-230.
63. Cline KK, Mcdermott MT, Mccreery RL. Anomalously slow electron transfer at ordered graphite electrodes: influence of electronic factors and reactive sites. *J Phys Chem*. 1994;98(20): 5314-5319.

64. McCreery RL. Advanced carbon electrode materials for molecular electrochemistry. *Chem Rev*. 2008;108(7):2646-2687.
65. Podyacheva OY, Cherepanova SV, Romanenko AI, et al. Nitrogen doped carbon nanotubes and nanofibers: composition, structure, electrical conductivity and capacity properties. *Carbon*. 2017;122:475-483.
66. Wiggins-Camacho JD, Stevenson KJ. Effect of nitrogen concentration on capacitance, density of states, electronic conductivity, and morphology of N-doped carbon nanotube electrodes. *J Phys Chem C*. 2009;113(44):19082-19090.
67. Qi X, Huang K, Wu X, et al. Novel fabrication of N-doped hierarchically porous carbon with exceptional potassium storage properties. *Carbon*. 2018;131:79-85.
68. Yang J, Ju Z, Jiang Y, et al. Enhanced capacity and rate capability of nitrogen/oxygen dual-doped hard carbon in capacitive potassium-ion storage. *Adv Mater*. 2018;30(4):1700104.
69. Yuan CQ, Liu XH, Jia MY, Luo ZX, Yao JN. Facile preparation of N- and O-doped hollow carbon spheres derived from poly(*o*-phenylenediamine) for supercapacitors. *J Mater Chem A*. 2015;3(7):3409-3415.
70. Li D, Ren X, Ai Q, et al. Facile fabrication of nitrogen-doped porous carbon as superior anode material for potassium-ion batteries. *Adv Energy Mater*. 2018;8(34):1802386.
71. Yang W, Zhou J, Wang S, et al. Freestanding film made by necklace-like N-doped hollow carbon with hierarchical pores for high-performance potassium-ion storage. *Energy Environ Sci*. 2019;12(5):1605-1612.
72. Xu F, Zhai Y, Zhang E, et al. Ultrastable surface-dominated pseudocapacitive potassium storage enabled by edge-enriched N-doped porous carbon nanosheets. *Angew Chem Int Ed*. 2020;59(44):19460-19467.
73. Xu Y, Zhang C, Zhou M, et al. Highly nitrogen doped carbon nanofibers with superior rate capability and cyclability for potassium ion batteries. *Nat Commun*. 2018;1(9):1720.
74. Zhang W, Cao Z, Wang W, et al. A site-selective doping strategy of carbon anodes with remarkable K-ion storage capacity. *Angew Chem Int Ed*. 2020;59(11):4448-4455.
75. Chang XQ, Zhou XL, Ou XW, Lee CS, Zhou JW, Tang YB. Ultrahigh nitrogen doping of carbon nanosheets for high capacity and long cycling potassium ion storage. *Adv Energy Mater*. 2019;9(47):1902672.
76. Liu Y, Dai H, Wu L, et al. A large scalable and low-cost sulfur/nitrogen dual-doped hard carbon as the negative electrode material for high-performance potassium-ion batteries. *Adv Energy Mater*. 2019;9(34):1901379.
77. Liu Q, Han F, Zhou J, et al. Boosting the potassium-ion storage performance in soft carbon anodes by the synergistic effect of optimized molten salt medium and N/S dual-doping. *ACS Appl Mater Interfaces*. 2020;12(18):20838-20848.
78. Lu C, Sun Z, Yu L, et al. Enhanced kinetics harvested in heteroatom dual-doped graphitic hollow architectures toward high rate printable potassium-ion batteries. *Adv Energy Mater*. 2020;10(28):2001161.
79. Xia G, Wang C, Jiang P, Lu J, Diao J, Chen Q. Nitrogen/oxygen co-doped mesoporous carbon octahedrons for high-performance potassium-ion batteries. *J Mater Chem A*. 2019;7(19):12317-12324.
80. Cui RC, Xu B, Dong HJ, Yang CC, Jiang Q. N/O dual-doped environment-friendly hard carbon as advanced anode for potassium-ion batteries. *Adv Sci*. 2020;7(5):1902547.
81. Lu J, Wang C, Yu H, et al. Oxygen/fluorine dual-doped porous carbon nanopolyhedra enabled ultrafast and highly stable potassium storage. *Adv Funct Mater*. 2019;29(49):1906126.
82. Wang H, Yang G, Chen Z, et al. Nitrogen configuration dependent holey active sites toward enhanced K^+ storage in graphite foam. *J Power Sources*. 2019;419:82-90.
83. Karlicky F, Datta KKR, Otyepka M, Zboril R. Halogenated graphenes: rapidly growing family of graphene derivatives. *ACS Nano*. 2013;7(8):6434-6464.
84. Zhang WC, Liu YJ, Guo ZP. Approaching high-performance potassium-ion batteries via advanced design strategies and engineering. *Sci Adv*. 2019;5(5):eaav7412.
85. Wang L, Jia JJ, Wu Y, Niu KM. Antimony/reduced graphene oxide composites as advanced anodes for potassium ion batteries. *J Appl Electrochem*. 2018;48(10):1115-1120.
86. Wang H, Wu X, Qi XJ, Zhao W, Ju ZC. Sb nanoparticles encapsulated in 3D porous carbon as anode material for lithium-ion and potassium-ion batteries. *Mater Res Bull*. 2018;103:32-37.
87. Sultana I, Rahman MM, Liu J, et al. Antimony-carbon nanocomposites for potassium-ion batteries: insight into the failure mechanism in electrodes and possible avenues to improve cyclic stability. *J Power Sources*. 2019;413:476-484.
88. He XD, Liu ZH, Liao JY, et al. Three-dimensional macroporous antimony@carbon composite as a high-performance anode material for potassium-ion batteries. *J Mater Chem A*. 2019;7(16):9629-9637.
89. Liu Q, Fan L, Ma R, et al. Super long-life potassium-ion batteries based on an antimony@carbon composite anode. *Chem Commun*. 2018;54(83):11773-11776.
90. Huang K, Xing Z, Wang L, et al. Direct synthesis of 3D hierarchically porous carbon/Sn composites via in situ generated NaCl crystals as templates for potassium-ion batteries anode. *J Mater Chem A*. 2018;6(2):434-442.
91. Yu Y, Cheng X, Li D, Wu Y, Xu R. Bismuth nanospheres embedded in three-dimensional (3D) porous graphene frameworks as high performance anodes for sodium- and potassium-ion batteries. *J Mater Chem A*. 2019;7(9):4913-4921.
92. Yu Q, Jiang B, Hu J, et al. Metallic octahedral $CoSe_2$ threaded by N-doped carbon nanotubes: a flexible framework for high-performance potassium-ion batteries. *Adv Sci*. 2018;5(10):1800782.
93. Lei K, Li F, Mu C, et al. High K-storage performance based on the synergy of dipotassium terephthalate and ether-based electrolytes. *Energy Environ Sci*. 2017;10(2):552-557.
94. Shen Q, Jiang PJ, He HC, Chen CM, Liu Y, Zhang M. Encapsulation of $MoSe_2$ in carbon fibers as anodes for potassium ion batteries and nonaqueous battery-supercapacitor hybrid devices. *Nanoscale*. 2019;11(28):13511-13520.
95. Wang W, Jiang B, Qian C, et al. Pistachio-shuck-like $MoSe_2$/C core/shell nanostructures for high-performance potassium-ion storage. *Adv Mater*. 2018;30(30):1801812.
96. Yu QY, Hu J, Qian C, Gao YZ, Wang W, Yin GP. CoS/N-doped carbon core/shell nanocrystals as an anode material for potassium-ion storage. *J Solid State Electrochem*. 2019;23(1):27-32.

97. Chen C, Yang Y, Tang X, Qiu R, Zhang M. Graphene-encapsulated FeS_2 in carbon fibers as high reversible anodes for Na^+/K^+ batteries in a wide temperature range. *Small*. 2019;15(10):1804740.
98. Zhao Y, Zhu J, Ong SJH, et al. High-rate and ultralong cycle-life potassium ion batteries enabled by in situ engineering of yolk-shell FeS_2@C structure on graphene matrix. *Adv Energy Mater*. 2018;8(36):1802565.
99. Xie J, Zhu Y, Zhuang N, et al. Rational design of metal organic framework-derived FeS_2 hollow nanocages@reduced graphene oxide for K-ion storage. *Nanoscale*. 2018;10(36):17092-17098.
100. Jia B, Zhao Y, Qin M, et al. Multirole organic-induced scalable synthesis of a mesoporous MoS_2-monolayer/carbon composite for high-performance lithium and potassium storage. *J Mater Chem A*. 2018;6(24):11147-11153.
101. Mao M, Cui C, Wu M, et al. Flexible ReS_2 nanosheets/N-doped carbon nanofibers-based paper as a universal anode for alkali (Li, Na, K) ion battery. *Nano Energy*. 2018;45:346-352.
102. Lakshmi V, Chen Y, Mikhaylov AA, et al. Nanocrystalline SnS_2 coated onto reduced graphene oxide: demonstrating the feasibility of a non-graphitic anode with sulfide chemistry for potassium-ion batteries. *Chem Commun*. 2017;53(59):8272-8275.
103. Chen Z, Yin DG, Zhang M. Sandwich-like MoS_2@SnO_2@C with high capacity and stability for sodium/potassium ion batteries. *Small*. 2018;14(17):1703818.
104. Bai J, Xi B, Mao H, et al. One-step construction of N,P-codoped porous carbon sheets/CoP hybrids with enhanced lithium and potassium storage. *Adv Mater*. 2018;30(35):1802310.
105. Verma R, Didwal PN, Ki HS, Cao GZ, Park CJ. SnP_3/carbon nanocomposite as an anode material for potassium-ion batteries. *ACS Appl Mater Interfaces*. 2019;11(30):26976-26984.
106. Yang F, Gao H, Hao J, et al. Yolk-shell structured FeP@C nanoboxes as advanced anode materials for rechargeable lithium-/potassium-ion batteries. *Adv Funct Mater*. 2019;29(16):1808291.
107. Tan Q, Li P, Han K, et al. Chemically bubbled hollow Fe_xO nanospheres anchored on 3D N-doped few-layer graphene architecture as a performance-enhanced anode material for potassium-ion batteries. *J Mater Chem A*. 2019;7(2):744-754.
108. Liu CL, Luo SH, Huang HB, Zhai YC, Wang ZW. Direct growth of MoO_2/reduced graphene oxide hollow sphere composites as advanced anode materials for potassium-ion batteries. *ChemSusChem*. 2019;12(4):873-880.
109. Zhao H, Zhi C, Shuangshuang D, Changmiao C, Ming Z. Enhanced electrochemical properties of SnO_2-graphene-carbon nanofibers tuned by phosphoric acid for potassium storage. *Nanotechnology*. 2018;29(37):375702.
110. Jin T, Li H, Li Y, Jiao L, Chen J. Intercalation pseudocapacitance in flexible and self-standing V_2O_3 porous nanofibers for high-rate and ultra-stable K ion storage. *Nano Energy*. 2018;50:462-467.
111. Sultana I, Rahman MM, Mateti S, Ahmadabadi VG, Glushenkov AM, Chen Y. K-ion and Na-ion storage performances of Co_3O_4-Fe_2O_3 nanoparticle-decorated super P carbon black prepared by a ball milling process. *Nanoscale*. 2017;9(10):3646-3654.
112. Wu H, Yu Q, Lao CY, et al. Scalable synthesis of VN quantum dots encapsulated in ultralarge pillared N-doped mesoporous carbon microsheets for superior potassium storage. *Energy Stor Mater*. 2019;18:43-50.
113. Li D, Zhu M, Chen L, et al. Sandwich-like $FeCl_3$@C as high-performance anode materials for potassium-ion batteries. *Adv Mater Interfaces*. 2018;5(15):1800606.
114. Wu Y, Hu S, Xu R, et al. Boosting potassium-ion battery performance by encapsulating red phosphorus in free-standing nitrogen-doped porous hollow carbon nanofibers. *Nano Lett*. 2019;19(2):1351-1358.
115. Tong Z, Yang R, Wu S, et al. Surface-engineered black niobium oxide@graphene nanosheets for high-performance sodium-/potassium-ion full batteries. *Small*. 2019;15(28):1901272.
116. Su DS, Schlögl R. Nanostructured carbon and carbon nanocomposites for electrochemical energy storage applications. *ChemSusChem*. 2010;3(2):136-168.
117. Mombeshora ET, Nyamori VO. A review on the use of carbon nanostructured materials in electrochemical capacitors. *Int J Energy Res*. 2015;39(15):1955-1980.
118. Wu X, Lam CWK, Wu N, et al. Multiple templates fabrication of hierarchical porous carbon for enhanced rate capability in potassium-ion batteries. *Mater Today Energy*. 2019;11:182-191.
119. Wang G, Xiong X, Xie D, et al. Chemically activated hollow carbon nanospheres as a high-performance anode material for potassium ion batteries. *J Mater Chem A*. 2018;6(47):24317-24323.
120. Mahmood A, Li S, Ali Z, et al. Ultrafast sodium/potassium-ion intercalation into hierarchically porous thin carbon shells. *Adv Mater*. 2019;31(2):1805430.
121. Li Y, Yang C, Zheng F, et al. Design of TiO_2eC hierarchical tubular heterostructures for high performance potassium ion batteries. *Nano Energy*. 2019;59:582-590.
122. Liu L, Chen Y, Xie Y, Tao P, Li Q, Yan C. Understanding of the ultrastable K-ion storage of carbonaceous anode. *Adv Funct Mater*. 2018;28(29):1801989.
123. Li P, Hwang JY, Park SM, Sun YK. Superior lithium/potassium storage capability of nitrogen-rich porous carbon nanosheets derived from petroleum coke. *J Mater Chem A*. 2018;6(26):12551-12558.
124. Li Y, Zhong W, Yang C, et al. N/S codoped carbon microboxes with expanded interlayer distance toward excellent potassium storage. *Chem Eng J*. 2019;358:1147-1154.
125. Li Y, Yang C, Zheng F, et al. High pyridine N-doped porous carbon derived from metal-organic frameworks for boosting potassium-ion storage. *J Mater Chem A*. 2018;6(37):17959-17966.
126. Chu J, Wang WA, Feng J, et al. Deeply nesting zinc sulfide dendrites in tertiary hierarchical structure for potassium ion batteries: enhanced conductivity from interior to exterior. *ACS Nano*. 2019;13(6):6906-6916.
127. Wei Z, Wang D, Li M, et al. Fabrication of hierarchical potassium titanium phosphate spheroids: a host material for sodium-ion and potassium-ion storage. *Adv Energy Mater*. 2018;8(27):1801102.
128. Gan Q, Xie J, Zhu Y, et al. Sub-20 nm carbon nanoparticles with expanded interlayer spacing for high-performance potassium storage. *ACS Appl Mater Interfaces*. 2019;11(1):930-939.

129. Zhang H, Luo C, He H, et al. Nano-size porous carbon spheres as a high-capacity anode with high initial coulombic efficiency for potassium-ion batteries. *Nanoscale Horiz*. 2020;5(5):895-903.
130. Bin DS, Chi ZX, Li Y, et al. Controlling the compositional chemistry in single nanoparticles for functional hollow carbon nanospheres. *J Am Chem Soc*. 2017;139(38):13492-13498.
131. Xu F, Ding B, Qiu Y, Dong R, Zhuang W, Xu X. Generalized domino-driven synthesis of hollow hybrid carbon spheres with ultrafine metal nitrides/oxides. *Matter*. 2020;3(1):246-260.
132. Liu J, Kopold P, Wu C, van Aken PA, Maier J, Yu Y. Uniform yolk-shell Sn_4P_3@C nanospheres as high-capacity and cycle-stable anode materials for sodium-ion batteries. *Energy Environ Sci*. 2015;8(12):3531-3538.
133. Liu Y, Yang C, Pan Q, et al. Nitrogen-doped bamboo-like carbon nanotubes as anode material for high performance potassium ion batteries. *J Mater Chem A*. 2018;6(31):15162-15169.
134. Xu F, Qiu Y, Jiang G, et al. Unraveling the correlation between structures of carbon nanospheres derived from polymeric spheres and their electrochemical performance to achieve high-rate supercapacitors. *Macromol Rapid Commun*. 2019;40(17):1800770.
135. Zhang HH, He HN, Luan JY, Huang XB, Tang YG, Wang HY. Adjusting the yolk-shell structure of carbon spheres to boost the capacitive K^+ storage ability. *J Mater Chem A*. 2018;6(46):23318-23325.
136. Zhang X, Deng YK, Wang YL, Zhan L, Yang SB, Song Y. Nanofibers with MoS_2 nanosheets encapsulated in carbon as a binder-free anode for superior lithium storage. *New Carbon Mater*. 2018;33(6):554-561.
137. Xiong PX, Zhao XX, Xu YH. Nitrogen-doped carbon nanotubes derived from metal-organic frameworks for potassium-ion battery anodes. *ChemSusChem*. 2018;11(1):202-208.
138. Zhang WM, Miao WF, Liu XY, Li L, Yu Z, Zhang QH. High-rate and ultralong-stable potassium-ion batteries based on antimony-nanoparticles encapsulated in nitrogen and phosphorus co-doped mesoporous carbon nanofibers as an anode material. *J Alloys Compd*. 2018;769:141-148.
139. Li W, Zeng L, Yang Z, et al. Free-standing and binder-free sodium-ion electrodes with ultralong cycle life and high rate performance based on porous carbon nanofibers. *Nanoscale*. 2014;6(2):693-698.
140. Wang SQ, Xia L, Yu L, Zhang L, Wang HH, Lou XW. Free-standing nitrogen-doped carbon nanofiber films: integrated electrodes for sodium-ion batteries with ultralong cycle life and superior rate capability. *Adv Energy Mater*. 2016;6(7):1502217.
141. Han JQ, Lu KY, Yue YY, et al. Synthesis and electrochemical performance of flexible cellulose nanofiber-carbon nanotube/natural rubber composite elastomers as supercapacitor electrodes. *New Carbon Mater*. 2018;33(4):341-350.
142. Adams RA, Syu JM, Zhao YP, Lo CT, Varma A, Pol VG. Binder-free N- and O-rich carbon nanofiber anodes for long cycle life K-ion batteries. *ACS Appl Mater Interfaces*. 2017;9(21):17872-17881.
143. Zhao XX, Xiong PX, Meng JF, Liang YQ, Wang JW, Xu YH. High rate and long cycle life porous carbon nanofiber paper anodes for potassium-ion batteries. *J Mater Chem A*. 2017;5(36):19237-19244.
144. Wang L, Wei K, Zhang P, et al. Porous CoC_2O_4/graphene oxide nanocomposite for advanced potassium-ion storage. *J Nanosci Nanotechnol*. 2019;19(6):3610-3615.
145. Wu X, Zhao W, Wang H, et al. Enhanced capacity of chemically bonded phosphorus/carbon composite as an anode material for potassium-ion batteries. *J Power Sources*. 2018;378:460-467.
146. Wang H, Xing Z, Hu Z, et al. Sn-based submicron-particles encapsulated in porous reduced graphene oxide network: advanced anodes for high-rate and long life potassium-ion batteries. *Appl Mater Today*. 2019;15:58-66.
147. Wang H, Wang L, Wang L, et al. Phosphorus particles embedded in reduced graphene oxide matrix to enhance capacity and rate capability for capacitive potassium-ion storage. *Chem Eur J*. 2018;24(52):13897-13902.
148. Yao Q, Zhang J, Shi X, et al. Rational synthesis of two-dimensional G@porous FeS_2@C composite as high-rate anode materials for sodium/potassium ion batteries. *Electrochim Acta*. 2019;307:118-128.
149. Zhang W, Yan Y, Xie Z, et al. Engineering of nanonetwork-structured carbon to enable high-performance potassium-ion storage. *J Colloid Interface Sci*. 2020;561:195-202.
150. Li H, Cheng Z, Zhang Q, et al. Bacterial-derived, compressible, and hierarchical porous carbon for high-performance potassium-ion batteries. *Nano Lett*. 2018;18(11):7407-7413.
151. Ge J, Fan L, Wang J, et al. $MoSe_2$/N-doped carbon as anodes for potassium-ion batteries. *Adv Energy Mater*. 2018;8(29):1801477.
152. Jian Z, Hwang S, Li Z, et al. Hard-soft composite carbon as a long-cycling and high-rate anode for potassium-ion batteries. *Adv Funct Mater*. 2017;27(26):1700324.
153. Lei Y, Han D, Dong J, et al. Unveiling the influence of electrode/electrolyte interface on the capacity fading for typical graphite-based potassium-ion batteries. *Energy Stor Mater*. 2020;24:319-328.

AUTHOR BIOGRAPHIES

Tianlai Wu received his bachelor degree in materials science and engineering from South China Agricultural University in 2019. He is currently a master degree candidate in the College of Materials and Energy at South China Agricultural University, China, under the supervision of Prof. Yeru Liang. His research focuses on carbon-based energy materials and the improvement of alkali-metal ion batteries.

Weicai Zhang received his bachelor degree from Dongguan University of Technology in 2017. He is currently a Ph.D. candidate in the College of Materials and Energy at South China Agricultural University, China, under the supervision of Prof. Yingliang Liu and Prof. Yeru Liang. His research

includes the design and improvement of alkali-metal ion battery and solid-state lithium battery.

Jiaying Yang received her bachelor degree from Northeast Forestry University in 2019. She is currently a master degree candidate in the School of Materials Science and Engineering, Northwestern Polytechnical University, China, under the supervision of Prof. Fei Xu. Her research interest focuses on the design and synthesis of hollow carbon spheres and their applications in energy storage.

Fei Xu received his bachelor (2009) and Ph.D. (2015) degrees from Sun Yat-sen University. Currently, he is an associate professor in the School of Materials Science and Engineering, Northwestern Polytechnical University. He worked at the Institute for Molecular Science, Japan (2012–2014), and then the Dresden University of Technology, Germany (2018–2020), as an Alexander von Humboldt Fellow. His research interests include the design, synthesis, and functional exploration of molecularly designed porous polymer/carbon architectures and their composites for challenging energy and environmental issues.

Yeru Liang received his bachelor (2008) and Ph.D. (2013) degrees from Sun Yat-sen University. Currently, he is a professor in the College of Materials and Energy at South China Agricultural University. His research interests focus on engineering porous carbons, carbon-based composite, and functional biomass-based materials for electrochemical energy storage and adsorption.

How to cite this article: Wu T, Zhang W, Yang J, et al. Architecture engineering of carbonaceous anodes for high-rate potassium-ion batteries. *Carbon Energy*. 2021;1–28.
https://doi.org/10.1002/cey2.99